R. & M. No. 3718


MINISTRY OF DEFENCE (PROCUREMENT EXECUTIVE)

AERONAUTICAL RESEARCH COUNCIL

REPORTS AND MEMORANDA

# An Analysis of the Drag of Two Annular Aerofoils

By C. YOUNG

Aerodynamics Dept., R.A.E., Farnborough

LONDON: HER MAJESTY'S STATIONERY OFFICE

1973

PRICE £2·25 NET

# An Analysis of the Drag of Two Annular Aerofoils

By C. YOUNG

Aerodynamics Dept., R.A.E., Farnborough

*Reports and Memoranda No.* 3718*
June, 1971

**Summary**

An analysis of the drag and pressure measurements made in subsonic wind-tunnel tests on two annular aerofoils is described. The relation between the design pressure distribution in incompressible flow and the pressure distribution on the aerofoil at high speed, is discussed.

An attempt has also been made to see what changes in the flow field are associated with the drag rise and whether the drag-rise Mach number can be predicted by methods similar to those used for ordinary aerofoils and bodies of revolution.

A comparison has been made of the measurements on a two-dimensional aerofoil and the annular aerofoils; no significant differences in the structure of local regions of supersonic flow were found at Mach numbers near the drag rise.

* Replaces RAE Technical Report No. 71126–ARC No. 33 662

LIST OF CONTENTS

## 1. Introduction

This report presents an analysis of the results from some wind-tunnel tests on three annular aerofoils[1]. The tests were made over a range of subsonic Mach numbers and mass-flow ratios and included measurements of the surface pressure distribution and drag coefficient.

The investigation reported in Ref 1 formed part of a wider programme of research into the aerodynamic problems associated with high bypass-ratio engines and was mainly concerned with two related problems in the design of the fan cowl. One main objective of the experimental work was to determine whether the conventional method of testing an intake on a 'pipe' rig instead of a complete cowl was still valid for the new range of geometries. This was achieved by testing a cowl whose forebody shape was the same as that of an intake tested on the B5 'pipe' rig at ARA[10]. The differences in the pressure distributions were fairly small at low speed but became much greater when there were extensive regions of supercritical flow on the forebody. In particular, the shock wave was further back on the complete cowl at all mass flow ratios. It was also conjected that the drag-rise Mach number of the complete cowl would be lower than on the intake because of the higher suction levels but an unrepresentative afterbody on the cowl led to some peculiar characteristics in the pressure distribution and no firm conclusions could be drawn from a comparison of the measured drag levels. More consideration is given to this point in Section 2.3.1.

A second objective of the experimental work was to provide data suitable for comparison with various theoretical methods of predicting the flow around annular aerofoils. A linearised and a non-linearised method[7] were used to calculate the pressure distribution on the cowls. The agreement between the measured pressure distribution and that predicted by the non-linearised theory was good, but the linearised theory failed at high Mach number. The use of such calculation methods in the design of improved cowl shapes was not discussed.

In the analysis presented in Ref 1, little attention was given to the actual performance of the cowls, or to how these measurements could be utilised in the design of better shapes. However, the cowl shapes which were tested were intended to investigate the value of designing cowls to have 'peaky' pressure distributions of the type which have been found attractive for two-dimensional aerofoils[2]. The design methods available at the time were relatively crude, but the cowls did develop significant regions of supercritical flow. The purpose of the present report is to analyse the experimental results in some detail in the hope of recognising the important features of these cowls. Whilst it cannot be expected that new design rules can be formulated on the basis of measurements on just three cowl shapes, it does appear that some useful conclusions can be drawn about the drag characteristics of the cowls and certain features of their pressure distribution.

Section 2.2 is mainly concerned with the relation between the pressure distributions on the cowl at low and high speed. This is an essential part of the analysis since only at low speed can the pressure distribution be calculated theoretically with any certainty, and it is important to establish if there are any features in the design pressure distribution which can be related to the extent and behaviour of the supercritical flow region at speeds near the drag-rise Mach number. The conclusions drawn from this part of the analysis must necessarily be somewhat tentative since there is a lack of detailed measurements on annular aerofoils and only two cowls, for which a comprehensive set of results are available, have been considered.

The drag measurements are discussed in Section 2.3. The various contributions to the total drag are examined in an attempt to relate features of the flow field to the drag rise. The prediction of the drag-rise Mach number from the incompressible pressure distribution is also attempted.

The performance of an engine cowl can also be measured in terms of the radial-force coefficient which corresponds to the lift coefficient of ordinary aerofoils. The measured radial-force coefficients are discussed in Sections 2.4 and 3.

The design of modern cowl shapes has relied, to a great extent, on advances made in the design of two-dimensional aerofoils. The measurements made on the cowls are compared with those made on a two-dimensional aerofoil of similar shape and thickness in Section 3. Some consideration is given to the structure of regions of local supersonic flow on two-dimensional and axisymmetric bodies, since it has been conjectured that there may be significant differences. In fact, the essential difference between

two-dimensional and annular aerofoils of similar profile seems to lie in the lower local velocities on the outer surface of the annular aerofoil, which implies a correspondingly higher critical Mach number and delayed drag-rise.

## 2. Analysis of the Experimental Results

### 2.1. Preliminary Comments

The analysis that has been made on the results from the wind-tunnel tests has been restricted to the measurements made[1] on cowls 2 and 3. Cowl 1 has not been specifically included because it had a considerably thicker and longer forebody than the other cowls. Furthermore, this cowl behaved unusually at high speed, when the shock on the forebody interacted with a region of increased suction just aft of the crest. The results from the tests on cowl 1, however, have not been entirely ignored and have been considered in making some general conclusions.

Part of the analysis is concerned with explaining why cowls 2 and 3, which had similar forebody dimensions, should behave so differently. For example, cowl 2 had a lower drag-rise Mach number than cowl 3 and also exhibited a fairly severe drag creep.

A full description of the design of the cowls and the experimental technique has already been given[1] but the main features of the experimental rig and the cowls are briefly described below.

A simplified drawing of the cowl rig, which was installed in the R.A.E. 8 ft × 6 ft transonic tunnel, is shown in Fig. 1. The cowls, which had a highlight diameter of 0·305 m, were connected to the balance by three thin support struts. Two of these struts carried the pressure tubes from the cowl to the sting while the third strut supported a rake of 17 pitot tubes and one static-pressure tube from which the mass flow through the cowl was determined. The flow at the cowl exit was surveyed by another pitot rake. The main rake consisted of 20 pitot tubes and one static-pressure tube but a further six pitot tubes, offset from the main rake in the region of the trailing edge, were added later. This rake was used to measure the external drag of the cowl.

The flow through the cowl was varied by using a screen which took the form of two 'fans' each with eighteen tapered arms of rectangular cross section. The front 'fan' was fixed and the rear fan was set with its arms either directly behind, or in between those of the front 'fan'. A thin 'fan' with half the blockage of the other two was also used.

Cowls 2 and 3 were designed as complete cowls using an eight point linearised method. The design mass-flow ratio for both cowls was 0·8 though neither cowl was tested at this value. Cowl 2 was designed to have a sonic roof-top pressure distribution at a Mach number of 0·75. The cowl had an 871/322* forebody, a leading-edge radius of 2·385 per cent chord and the crest was 37 per cent chord.

Cowl 3 had an 884/314 forebody and was designed to have a 'peaky' pressure distribution with a peak local Mach number of about 1·2 at a free-stream Mach number of 0·78. The peak was followed by a constant-velocity region which was sonic at the design Mach number. The leading-edge radius of the cowl was 1·802 per cent chord and the crest was at 35·5 per cent chord.

### 2.2. Local Mach Number Distributions

The aim of this Section is to see if, when there are extensive regions of supercritical flow, the development of the pressure distribution on the cowl at high speed can be related to any features of the pressure distribution at low speed.

For two-dimensional aerofoils empirical relations have been developed for calculating the pressure distribution on an aerofoil at high speed even when shocks are present[2]. The long term objectives of research on cowls are similar, but there is not the same wealth of experimental data as for two-dimensional aerofoils, and at this stage only a qualitative approach seems possible.

The pressure distributions measured on cowls 2 and 3 at a Mach number of 0·3 and at two mass-flow

* i.e. the ratio of highlight diameter to maximum diameter of the external shape was 0·871, and the ratio of the forebody length to maximum diameter was 0·322. For all three cowls, the chord length was equal to the highlight diameter.

ratios are shown in Figs. 2 and 3. An abscissa of $\sqrt{x/c}$ has been used in these figures to emphasise the differences in the distribution near the leading edge of the cowls.

Two main differences in the pressure distributions on the cowls are apparent.

(1) The peak suction level is higher on cowl 3.

(2) The overall suction level behind the peak, and especially on the afterbody, is higher on cowl 2.

The local Mach number distributions on the outer surface of the cowls at free-stream Mach numbers of 0·7 and above are shown in Figs. 4 to 11.

The most noticeable feature of these distributions is that the shock wave on cowl 3 is further forward, and in many cases weaker than the shock wave on cowl 2, for the same mass-flow ratio and free-stream Mach number. Also, cowl 3 retains the higher suction level at the peak throughout the range of Mach numbers and mass-flow ratios covered in these tests. These statements together imply that more isentropic recompression is achieved on cowl 3.

The shape of the peak on cowl 3 was not well defined in the design method used but it does seem that the peak is a good feature and indicates that improved cowl shapes can be designed on the basis of a well chosen 'peaky' pressure distribution.

The drag creep of cowl 2 was due to the rapid rearward movement of the shock wave with increasing Mach number. The shock wave moved back rapidly because of the higher overall suction levels behind the peak and on the afterbody.

Such an explanation can also be used to account for the difference in extent of the supersonic-flow region on a complete cowl and on an intake tested in isolation. The region of constant suction level behind the leading-edge peak is maintained for some distance behind the peak on a complete cowl; this plateau is then followed by an adverse pressure gradient to the trailing edge. In a pipe-rig test where the intake is followed by a long section of constant diameter, the suction level drops gradually behind the peak to a fairly low level. The shock wave moves back slowly though it gains in strength as the Mach number is increased. In the ARA tests[10], the drag-rise appears to occur when the shock wave has moved to about 80 per cent of the forebody length and is primarily due to the rapid increase in wave drag or loss of thrust on the cowl. The source of the wave drag is the loss of momentum at the shock which is transmitted to the intake by readjustments in the pressure distribution over the surface. After the drag-rise, the shock wave continues to move slowly back and reaches the end of the forebody at a considerably higher Mach number.

The shock wave moved back more rapidly on the complete cowl than on the corresponding intake. The drag-rise occurred just after the shock passed over the crest and was due initially to a loss of thrust on the cowl but this was quickly followed in the present tests by a shock-induced boundary-layer separation (*see* Section 2.3).

The variation of the local Mach number at the peak with intake velocity ratio is shown in Figs. 12 and 13. The peak local Mach number increased as the free-stream Mach number increased until the latter reached a value of about 0·8. Further increases were very small beyond this and there was an indication that the peak local Mach number was decreasing at the lowest velocity ratio. This is similar to the Mach number 'freeze' observed on two-dimensional aerofoils.

There is no doubt that the use of a 'peaky' pressure distribution in the design of cowl 3 was beneficial, but merely from these results, it is impossible to say how the optimum 'peaky' pressure distribution can be designed with regard to the peak suction level, the width of the peak and its behaviour with changes of mass-flow ratio. More experiments are needed on 'peaky' sections to understand fully the relation between the low-speed and high-speed pressure distributions. The rearward movement of the shock may be influenced by the suction level behind the leading-edge peak, and to a certain extent, by the pressure distribution on the afterbody. The slightly lower suction level on cowl 3 appeared to retard the movement of the shock and a similar effect has been observed on intakes tested in isolation[10]. Further experimental evidence is needed to see if this feature can be exploited in the design of better cowl shapes.

### 2.3. Drag Measurements

The methods of predicting the drag-rise Mach number of an engine cowl in use at present are based on data from extensive tests of the N.A.C.A.-1 intake shape[11]. These methods work well for the N.A.C.A.-1

shapes since those profiles are geometrically similar but they are unlikely to be satisfactory for the current intake and cowl designs because these shapes are not related to the N.A.C.A.-1 profile and the design pressure distributions are different. Any new criteria that may be devised for the prediction of the drag-rise Mach number must therefore take into account the design pressure distribution as well as the cowl geometry. A different criterion may be required for complete cowls and isolated intakes as the behaviour of the supercritical flow region is different in the two cases.

In this section, the drag of cowl 3 is analysed in detail and various criteria examined which may lead to a better method of predicting the drag-rise of cowls.

The drag coefficients, of the external surface only, measured on cowls 2 and 3 are shown as a function of Mach number in Figs. 14 and 15. The reference area used in the definition of the drag coefficient is different to that used in Ref. 1; the approximate external surface area of the cowl ($2\pi r_i c$) has been used instead of the projected frontal area of the cowl, to keep the presentation consistent when the relation between cowls and aerofoils is discussed in Section 3.

The two main contributions to the total drag, the pressure drag and the skin-friction drag, have been analysed separately in order to understand the changes that occur in the flow field near the drag-rise Mach number.

The variation of the pressure drag, which includes the contributions from the internal and external surfaces, with Mach number for cowl 3 is shown in Figs. 16 to 19. The pressure drag was determined by graphically integrating the thrust and drag loops from the pressure distributions. The thrust and drag contributions are shown separately in addition to the total pressure drag.

As the mass-flow ratio decreases, the pressure drag becomes negative because the cowl must generate a thrust force to balance the momentum change in the approaching stream tube. This thrust force can also be calculated theoretically. The formula used, which is derived in the Appendix, is

$$C_T = \frac{2}{\gamma M^2}\left[1 - \left\{1 + \frac{\gamma - 1}{2}M^2\left(1 - \left(\frac{V_e}{V_0}\right)^2\right)\right\}^{3{\cdot}5}\right] + \frac{2V_e}{V_0}\left(1 - \frac{V_e}{V_0}\right)\left\{1 + \frac{\gamma - 1}{2}M^2\left(1 - \left(\frac{V_e}{V_0}\right)^2\right)\right\}^{2{\cdot}5},$$

where the subscript $e$ refers to conditions downstream of the trailing edge. The velocity ratio $V_e/V_0$ is related to the mass-flow ratio by

$$\frac{V_e}{V_0}\left[1 + \frac{\gamma - 1}{2}M^2\left(1 - \left(\frac{V_e}{V_0}\right)^2\right)\right]^{2{\cdot}5} = \mu\frac{A_i}{A_e}.$$

The values of $V_e/V_0$ used to calculate the theoretical thrust force shown in Figs. 16 to 19, are tabulated in Table 2. Quite close agreement between theory and experiment at low speeds was obtained but the measured thrust was considerably less than the theoretical values at Mach numbers above the drag-rise.

The measured values of the external drag coefficient was also shown in Figs. 16 to 19 for comparison.

The shape of some typical thrust and drag loops are shown in Figs. 20 to 22. At low speed, Fig. 20, the thrust and drag loops were approximately the same size. At a Mach number of 0·82, Fig. 21, the supercritical pressure distribution was favourable; the thrust was at a maximum and the total pressure drag had decreased slightly. This situation occurred when the shock wave had just passed over the crest of the cowl, Fig. 7. The size of the thrust loop decreased with further increases of Mach number, Fig. 22, and a second smaller drag loop appeared. The loss of thrust caused by the shock wave passing well beyond the crest had a greater effect on the total pressure drag than the appearance of the second drag loop. The drag-rise Mach number is therefore associated with an overall increase in the pressure drag caused by a considerable loss of thrust on the cowl.

The drag-rise Mach number of cowls 2 and 3 has been plotted against mass-flow ratio in Fig. 23. The Mach number at which the shock wave passed over the crest of the cowl is also shown. The shape of the curves is similar though the drag-rise occurred at a slightly higher Mach number. This is consistent with the shape of the thrust and drag loops since the shock can pass just over the crest before there is a serious reduction in the size of the thrust loop.

The shock wave on the cowl also causes thickening and eventually separation of the boundary layer. The calculated skin-friction coefficient on cowl 3 at a mass flow ratio of 0·77 and at Mach numbers between 0·80 and 0·86 are shown in Fig. 24. The calculation method used[4] predicted a separation in all cases. In practice there is no evidence of separation on the cowl at the lower Mach number, but the sudden forward movement of the predicted separation point between $M = 0{\cdot}82$ and $M = 0{\cdot}84$ does seem to correlate with the experimental variation of the trailing-edge pressure parameter, $\Delta$, with Mach number shown in Fig. 25. This trailing-edge pressure parameter defined by

$$\Delta = (1 - (p/H)_{TE})/(1 - p_0/H_0)$$

has proved useful in the study of the drag characteristics of two-dimensional aerofoils. An increase in the trailing-edge pressure parameter occurs when the flow near the trailing edge is affected by the growth of the upper-surface separation bubble.

The trailing-edge pressure parameter for cowl 3 increased after the drag-rise Mach number, indicating that the initial drag-rise is due to the loss of thrust on the cowl and a shock-induced boundary-layer separation of significant extent occurs at a slightly higher Mach number.

One unexplained feature of Fig. 25 is the rapid decrease in the trailing-edge pressure parameter just before the drag rise. Such a pronounced decrease has not been observed on two-dimensional aerofoils and its significance in this case is not understood.

2.3.1. *Comparison with intakes tested in isolation.* No direct comparison of the drag results for cowls 2 and 3 presented in this Report with those measured on an intake in isolation can be made, as no such intake has been tested. However, in Ref. 1, the drag measured on cowl 1 was compared with the drag measured on an intake which had the same forebody shape as the cowl[10]. This comparison was not conclusive because the afterbody of the cowl was not representative, but the comparison of the pressure distributions showed that the suction level on a complete cowl was higher than on the intake alone.

The shock wave on the intake was also weaker and further forward than on the cowl because there was no pressure gradient behind the forebody on the intake. Thus the drag-rise Mach number measured on an intake in isolation would normally be higher than that which would be measured on the intake with a representative afterbody. Boundary-layer separations on the isolated intake are certainly delayed and may be absent altogether and it is expected that the tests on the pipe rig will not give fully representative results above the drag-rise Mach number. In particular, the margin between drag-rise and flow separation for a complete cowl cannot be predicted with any confidence from such tests.

However, current designs for fan cowls have a larger chord to diameter ratio than cowl 1 so the technique of testing an isolated intake is more realistic. Theoretical calculations can also be made[7] to estimate the effect of adding the afterbody. At present these calculations can only be made at low Mach number but the application of the numerical methods now being developed to calculate the supercritical pressure distribution on two-dimensional aerofoils to axisymmetric bodies will permit this speed range to be increased.

2.3.2. *Estimation of the drag-rise Mach number.* The methods for predicting the drag-rise Mach number of aerofoils or bodies of revolution use a simple scaling of the calculated pressure coefficient at the crest. For two-dimensional aerofoils[5] a good estimate of the drag-rise Mach number is obtained by calculating the free-stream Mach number at which the local Mach number at the crest becomes 1·02, using the Kármen-Tsien compressibility factor. The same value of the local Mach number at the crest is also used for bodies of revolution[6] but the scaling in this case is done using the full Prandtl-Glauert transformation.

The development of a similar method for cowls would satisfy the conditions previously expressed that any new drag-rise criterion must take into account the cowl geometry and the shape of the pressure distribution. A computer program[7] has been used to see whether the criterion that the local Mach number at the crest of 1·02 can also be associated with the drag-rise for cowls. The calculations have shown, Fig. 26, that this criterion leads to a very pessimistic value of the drag-rise Mach number, Fig. 27, and that a local Mach number of about 1·1 would be more appropriate.

A purely empirical relation that gives better agreement with the measured drag-rise has also been used, Fig. 27. The calculated pressure coefficient at the crest in incompressible flow is scaled by a factor of $1/\beta$ to give a local Mach number of 1·2. This value was chosen from an analysis of the measured pressure distributions and is not likely to work for cowls with a chord to diameter ratio very different from unity. From an analysis of the data from the B5 pipe rig[10], for example, the drag-rise occurs when the local Mach number at the end of the forebody is about 0·93.

### 2.4. The Radial Force Coefficient

The aerodynamic force exerted by the flow around an annular aerofoil can be resolved into two components; a radial force component $F_R$, and an axial force component $F_X$. The axial force component is the drag and has been considered in Section 2.3. The radial force component is considered in this section.

The radial force is not so important in practice since in symmetric flow, the diametrically opposed components balance each other, but it is considered here, and in Section 3, as this force corresponds to the lift force of ordinary aerofoils.

The radial-force component, $C_R$, is defined as

$$C_R = F_R/\tfrac{1}{2}\rho V^2 c$$

where $F_R$ is the radial force per unit length of circumference.

The variation of the radial force coefficient obtained by graphically integrating the pressures with the velocity decrement, $1 - V_i/V_0$, is shown in Figs. 28 and 29. There was almost a linear variation over most of the Mach number range.

The radial force coefficient is shown as a function of Mach number in Figs. 30 and 31. The coefficient increased slowly until there was a significant amount of supercritical flow present, when the increase was more rapid. In nearly all cases the radial force coefficient increased with Mach number even beyond the drag-rise though the increase is less when separation has occurred and significant amounts of separation are likely to lead to a reduction in the radial force coefficient.

The relation between the measured external drag and the radial force coefficient is shown in Fig. 32. There is no recognisable pattern in the results for cowl 2 because of the drag creep associated with this cowl. The results for cowl 3, however, show a smooth variation up to the drag-rise Mach number. This figure is similar to Fig. 5–12 of Ref. 3, which was obtained from low-speed-tunnel tests of annular aerofoils in the early 1940's.

## 3. A Comparison between Two-dimensional and Annular Aerofoils

There are important differences between the flow about two-dimensional and annular aerofoils which must be investigated if the design rules now used for two-dimensional aerofoils can be fully exploited in engine cowl design. In this section, comparisons are made between the forces and pressure distributions on the cowls with those on a two-dimensional aerofoil of similar shape and thickness.

The aerofoil chosen, designated NPL 3131, was one of a series tested at NPL several years ago[12]. This aerofoil has a 13 per cent thick section with the maximum thickness at 41 per cent chord and a leading edge radius of 0·95 per cent chord. It was designed to have a sonic roof-top pressure distribution at the design conditions ($M = 0{\cdot}66, C_L = 0{\cdot}64, \alpha \simeq 3°$); at higher lift coefficients it was intended to develop a supercritical peak which happens to be intermediate between those of cowls 2 and 3.

The measured drag coefficient of the aerofoil is shown in Fig. 33 for angles of incidence of 3·4, 4·4 and 5·4 degrees. The drag-rise Mach number is considerably lower than that measured on the cowls.

The drag coefficient of the aerofoil at low speed is about twice that of the cowls. This is because the drag of the cowl is defined as the drag due to the outer surface only whilst the aerofoil drag includes the contributions from the upper and lower surfaces.

The variation of the lift coefficient of the aerofoil and the radial force coefficient of the cowls with Mach number is shown in Figs. 34 and 35. The lift coefficient of the aerofoil falls off rapidly with increases of Mach number above the drag-rise whereas the radial force coefficient of the cowls increases up to the highest Mach number of the tests.

The loss of lift on the aerofoil is associated with a substantial reduction of suction near the leading edge which is probably due to the small leading-edge radius, and, at Mach numbers above 0·78, with the appearance of a shock wave on the lower surface of the aerofoil. There is a small reduction in suction near the leading edge of the cowl at the high Mach numbers but this is more than compensated by higher suction levels over the rest of the cowl forebody.

Two typical pressure distributions measured on cowl 2 and the aerofoil are compared in Fig. 36. The suction levels on both surfaces of the cowl are lower than on the aerofoil even though the radial force and lift coefficients are similar. The lower mean velocity level on the cowl is due to the effect of camber[8] but the velocity increments due to the loading are similar in the two cases. Fig. 37 shows the pressure distributions on both cowls and the aerofoil just beyond their respective drag-rise Mach numbers. The pressure distributions are similar in shape but the difference in free stream Mach number is large.

### 3.1. Extent of the Supersonic region

It has been conjectured that the delayed drag-rise on cowls might be associated with differences in the shape and extent of the supersonic-flow region. Some calculations have been made for this purpose using the method of characteristics[9]. The calculations involved are fairly straightforward except in the axisymmetric case where an iteration is required to find the points where the characteristics of the opposite families intersect.

The calculated characteristic meshes and sonic lines for the three pressure distributions of Fig. 37 are shown in Figs. 38 to 43. The differences in the meshes for the two cowls and the aerofoil are fairly small; the supersonic regions extend to about the same distance from the surface in all cases, thus the drag-rise occurred when there was substantially the same amount of supercritical flow present.

The differences in the characteristic meshes occurred near the leading edge of the aerofoils. The characteristic lines were bent further forward in the axisymmetric case but this could be a consequence of the greater nose radii of the cowls. The slope of the sonic line is greater in the two-dimensional case so that initially the supersonic flow extends further from the surface of the aerofoil. This can also be seen in Fig. 44 where the two calculation methods have been applied to the same pressure distribution.

Although there is a high degree of similarity in the shapes of the characteristic meshes, there is a large difference in the free-stream Mach number at which these patterns occur. The region of supersonic flow on the aerofoil at a Mach number of 0·70 is about the same as that on cowl 3 at a Mach number of 0·84. This can be thought of in terms of the stream tubes being able to expand outwards more easily in axisymmetric flow than the streamlines in two-dimensional flow. A possible basis for comparing the behaviour of regions of supercritical flow on aerofoils and cowls is to make the comparison at a Mach number measured relative to the drag-rise Mach numbers of the respective bodies.

## 4. Conclusions

An analysis has been made of the results of some wind-tunnel tests on annular aerofoils. The purpose of the analysis was to investigate how large amounts of supercritical flow affect the performance of an annular aerofoil or engine cowl. Such an analysis is required if better cowls are to be designed using existing design methods.

Thin fan cowls are preferred for engines of high bypass ratio because of weight and drag considerations, and it seems likely that areas of supercritical flow will be present over most of the operating range of the cowl but, as all design methods are based on potential flow theory, the relation between the pressure distribution on the cowl at low and high speeds must be fully understood. The results for cowls 2 and 3 were analysed in Section 2.2 for this reason, but the conclusions reached must be regarded as tentative until more experimental evidence is available. There is little doubt, however, that a pressure distribution of the 'peaky' type is as beneficial for cowls as it is for ordinary aerofoils but from the measurements made on only two cowls it is not possible to determine what qualities this pressure distribution should have. More shapes need to be tested to explore the possible gains in performance that can be attained with more advanced section designs.

The contributions to the total drag of cowl 3 were analysed in Section 2.3. The drag-rise Mach number is associated with a considerable loss of thrust on the cowl immediately after the shock wave has passed over the crest. A severe boundary-layer separation occurs at a slightly higher Mach number. This is different from the mechanism of the drag-rise for intakes tested on a 'pipe' rig. Here, the drag-rise is due solely to the appearance of shock waves and boundary layer effects are delayed to a much higher Mach number. Thus the drag-rise Mach number for an intake that is to form the forebody of a short cowl may be overestimated, and the drag levels beyond the drag-rise will be underestimated. The methods of predicting the drag-rise Mach number of a two-dimensional aerofoil or body of revolution, by estimating the free-stream Mach number at which the local Mach number at the crest is 1·02, do not seem to work for cowls, and a local Mach number of about 1·1 gives a better estimate. A purely empirical relation was also developed.

The difference in the behaviour of cowls and ordinary aerofoils was investigated in Section 3. It was shown that there are no large differences in the structure of the supersonic flow region at Mach numbers near to the drag-rise, though the drag-rise of an ordinary aerofoil occurs at a much lower Mach number than on the corresponding annular aerofoil. This is mainly associated with differences in the low speed pressure distribution.

## LIST OF SYMBOLS

| | |
|---|---|
| $c$ | cowl or aerofoil chord length |
| $C_D$ | drag coefficient |
| $C_f$ | Skin-friction coefficient |
| $C_L$ | Lift coefficient |
| $C_p$ | Pressure coefficient |
| $C_R$ | Radial-force coefficient |
| $C_T$ | Thrust coefficient |
| $F_N$ | Thrust force |
| $F_R$ | Radial force |
| $F_X$ | Axial force |
| $H$ | Total pressure |
| $M$ | Mach number |
| $M_D$ | Drag-rise Mach number |
| $p$ | Static pressure |
| $r$ | Radial coordinate |
| $V$ | Velocity |
| $x$ | Axial coordinate |
| $z$ | Vertical coordinate |
| $\Delta$ | Trailing-edge pressure parameter |
| $\mu$ | Mass-flow ratio |
| $\rho$ | Density |
| $\beta$ | $\sqrt{1-M^2}$ |

*Subscripts*

| | |
|---|---|
| crest | Crest conditions |
| $e$ | Conditions downstream of the cowl trailing edge |
| $i$ | Inlet station |
| $L$ | Local conditions |
| $O$ | Free-stream conditions |
| peak | Peak-suction station |
| te | Trailing edge |

## REFERENCES


| *No.* | *Author(s)* | *Title, etc.* |
|---|---|---|
| 1 | C. Young .. .. .. | An investigation of annular aerofoils for turbofan engine cowls. A.R.C. R. & M. 3688 (1969). |
| 2 | H. H. Pearcey .. .. .. | The aerodynamic design of section shapes for swept wings. *Advances in Aeronautical Sciences*, Vol. 3, pp. 277–322, Pergamon Press, London (1962). |
| 3 | D. Küchemann and J. Weber | *Aerodynamics of propulsion* McGraw Hill (1952). |
| 4 | J. E. Green .. .. .. | The prediction of turbulent boundary-layer development in compressible flow. *J. Fluid Mech.*, Vol. 31, part 4 (1968). |
| 5 | J. E. Green .. .. .. | A method of estimating the drag-rise Mach number for two-dimensional aerofoil sections. R.Ae.Soc Transonic Data Memo 6407 (1964). |
| 6 | J. E. Green .. .. .. | A method for estimating drag-rise Mach number of smooth non-ducted axisymmetric bodies at zero incidence. R.Ae.Soc. Transonic Data Memo (in preparation). |
| 7 | C. Young .. .. .. | A computer program to calculate the pressure distribution on an annular aerofoil. A.R.C. C.P. 1217 (1971). |
| 8 | J. A. Bagley, N. B. Kirby and P. J. Marcer | A method of calculating the velocity distribution on annular aerofoils in incompressible flow. A.R.C. R. & M. 3146 (1958). |
| 9 | W. R. Sears (Editor) .. .. | *General theory of high speed aerodynamics, section G.* Oxford University Press, Oxford (1955). |
| 10 | M. J. Langley .. .. .. | Measurements of external drag and surface pressure distributions on six cowls designed for high subsonic Mach No. A.R.A. Model Test Note M 31/1 (1971). |
| 11 | R. Hetherington .. .. | *In*: High Reynolds Number Subsonic Aerodynamics. Paper 10: The aerodynamics of engine component design problems associated with large subsonic aircraft. Agard Lecture Series No. 37, June 1970. |
| 12 | R. Hetherington .. .. | The two-dimensional aerofoil tests in the 20″ × 8″ tunnel at the N.P.L.: Part 2 Aerofoil B H.S.A. Note Aero/681/44/1102 (1965). |

## APPENDIX

### The Calculation of the Thrust Force on the Cowl

In Section 2.3 it was stated that the thrust force on the cowl could be calculated theoretically using the momentum equation.

In a purely inviscid flow, the force experienced by the cowl must be equal to the change in momentum of the airstream between a station at infinity upstream and a downstream station, Fig. 45.

The change in momentum $\Delta M$ is,

$$\Delta M = p_0 A_0 + \rho_0 V_0^2 A_0 - p_0(A_0 - A_e) - p_e A_e - (\rho_0 V_0 A_0 - \rho_e V_e A_e)V_0 - \rho_e V_e^2 A_e$$

$$= A_e(p_0 - p_e) + \rho_e V_e A_e(V_0 - V_e);$$

hence

$$\frac{\Delta M}{\frac{1}{2}\rho_0 V_0^2 A_e} = \frac{p_0 - p_e}{\frac{1}{2}\rho_0 V_0^2} + 2\frac{\rho_e}{\rho_0}\frac{V_e}{V_0}\left(1 - \frac{V_e}{V_0}\right).$$

From the energy equation,

$$\frac{p_e}{p_0} = \left\{1 + \frac{\gamma - 1}{2}M^2\left(1 - \left(\frac{V_e}{V_0}\right)^2\right)\right\}^{3\cdot5}$$

and

$$\frac{\rho_e}{\rho_0} = \left\{1 + \frac{\gamma - 1}{2}M^2\left(1 - \left(\frac{V_e}{V_0}\right)^2\right)\right\}^{2\cdot5}.$$

The thrust force on the cowl $C_T$ becomes

$$C_T = \frac{\Delta M}{\frac{1}{2}\rho_0 V_0^2(2\pi r_i c)}$$

$$= \frac{A_e}{2\pi r_i c}\left\{\frac{2}{\gamma M^2}\left[1 - \left\{1 + \frac{\gamma - 1}{2}M^2\left(1 - \left(\frac{V_e}{V_0}\right)^2\right)\right\}^{3\cdot5} + \frac{2V_e}{V_0}\left(1 - \frac{V_e}{V_0}\right)\left\{1 + \frac{\gamma - 1}{2}M^2\left(1 - \left(\frac{V_e}{V_0}\right)^2\right)\right\}^{2\cdot5}\right\}\right.$$

The velocity $V_e$ can be related to the mass-flow ratio $\mu$ using the continuity equation,

$$\frac{V_e}{V_0} = \frac{\rho_0 A_0}{\rho_e A_e} = \frac{\rho_0}{\rho_e}\frac{A_0}{A_i}\frac{A_i}{A_e}$$

$$\frac{V_e}{V_0}\left[1 + \frac{\gamma - 1}{2}M^2\left(1 - \left(\frac{V_e}{V_0}\right)^2\right)\right]^{2\cdot5} = \mu\frac{A_i}{A_e}.$$

$V_e/V_0$ can be found from an iterative solution to this equation.

The area $A_e$ is also unknown. As a first approximation, the wake can be assumed to be cylindrical and the area at the trailing edge can be used but this gives values of the thrust coefficient which are too large. The thrust coefficients shown in Figs. 16 to 19 were based on an area obtained by calculating the radius of the stagnation streamtube at one chord length downstream of the trailing edge. This calculation was

made using the same mathematical model of the flow as in the computer program used to calculate the pressure distribution on an annular aerofoil[7].

The ratios of the radius of the stagnation streamtube to the trailing edge radius are listed in Table 1, and the values of the thrust coefficient using the trailing-edge area, and the area calculated from the streamlines are tabulated in Table 3. The values of $V_e/V_0$ used from the calculation of the thrust coefficient using the streamtube area are listed in Table 2.

TABLE 1

**The Ratio of the Radius of the Stagnation Streamtube $r_{stag}$, to the Trailing Edge Radius $r_{te}$**

| Mass flow ratio | $\frac{r_{stag}}{r_{te}}$ |
|---|---|
| ~0·77 | 0·946 |
| ~0·70 | 0·943 |
| ~0·63 | 0·940 |
| ~0·53 | 0·929 |

TABLE 2

**Values of $V_e/V_0$ used to Calculate the Thrust Coefficient using the Area from the Streamline Calculation**

| Mach number | Mass flow ratio | $\frac{V_e}{V_0}$ | Mach number | Mass flow ratio | $\frac{V_e}{V_0}$ |
|---|---|---|---|---|---|
| 0·3 | 0·76 | 0·9598 | 0·3 | 0·66 | 0·8331 |
| 0·5 | 0·76 | 0·9474 | 0·5 | 0·66 | 0·8082 |
| 0·7 | 0·76 | 0·9275 | 0·7 | 0·65 | 0·7485 |
| 0·75 | 0·77 | 0·9420 | 0·75 | 0·65 | 0·7326 |
| 0·8 | 0·78 | 0·9610 | 0·8 | 0·63 | 0·6836 |
| 0·82 | 0·77 | 0·9285 | 0·82 | 0·63 | 0·6759 |
| 0·84 | 0·77 | 0·9233 | 0·84 | 0·63 | 0·6679 |
| 0·86 | 0·77 | 0·9175 | 0·86 | 0·63 | 0·6597 |
| 0·3 | 0·71 | 0·8943 | 0·3 | 0·57 | 0·7308 |
| 0·5 | 0·70 | 0·8617 | 0·5 | 0·56 | 0·6869 |
| 0·7 | 0·70 | 0·8369 | 0·7 | 0·54 | 0·6086 |
| 0·75 | 0·70 | 0·8086 | 0·75 | 0·53 | 0·5794 |
| 0·8 | 0·70 | 0·7917 | 0·8 | 0·53 | 0·5626 |
| 0·82 | 0·69 | 0·7662 | 0·82 | 0·53 | 0·5555 |
| 0·84 | 0·69 | 0·7581 | 0·84 | 0·53 | 0·5483 |
| 0·86 | 0·69 | 0·7496 | 0·86 | 0·53 | 0·5410 |

TABLE 3

**Theoretical Values of the Thrust Coefficient**

| Mach number | Mass flow ratio | Thrust coefficient | | |
|---|---|---|---|---|
| | | Calculated using trailing edge area | Calculated using area from streamlines | Measured |
| 0·3 | 0·76 | −0·00480 | −0·00030 | −0·00035 |
| 0·5 | 0·76 | −0·00559 | −0·00043 | 0·00268 |
| 0·7 | 0·76 | −0·00729 | −0·00060 | 0·00243 |
| 0·75 | 0·77 | −0·00684 | −0·00033 | 0·00411 |
| 0·8 | 0·78 | −0·00641 | −0·00028 | 0·00150 |
| 0·82 | 0·77 | −0·00788 | −0·00042 | −0·00247 |
| 0·84 | 0·77 | −0·00827 | −0·00045 | −0·00414 |
| 0·86 | 0·77 | −0·00866 | −0·00049 | 0·00604 |
| 0·3 | 0·71 | −0·01158 | −0·00204 | −0·00185 |
| 0·5 | 0·70 | −0·01198 | −0·00306 | −0·00285 |
| 0·7 | 0·70 | −0·01508 | −0·00404 | −0·00385 |
| 0·75 | 0·70 | −0·01622 | −0·00448 | −0·00220 |
| 0·8 | 0·70 | −0·01758 | −0·00499 | −0·00468 |
| 0·82 | 0·69 | −0·01993 | −0·00636 | −0·00680 |
| 0·84 | 0·69 | −0·02062 | −0·00666 | −0·00410 |
| 0·86 | 0·69 | −0·02135 | −0·00699 | 0·00609 |
| 0·3 | 0·66 | −0·01535 | −0·00511 | −0·00324 |
| 0·5 | 0·66 | −0·01749 | −0·00594 | −0·00759 |
| 0·7 | 0·65 | −0·02336 | −0·00890 | −0·00917 |
| 0·75 | 0·65 | −0·02492 | −0·00966 | −0·01169 |
| 0·8 | 0·63 | −0·03080 | −0·01358 | −0·01423 |
| 0·82 | 0·63 | −0·03167 | −0·01407 | −0·01217 |
| 0·84 | 0·63 | −0·03258 | −0·01459 | −0·00576 |
| 0·86 | 0·63 | −0·03355 | −0·01516 | −0·00177 |
| 0·3 | 0·57 | −0·02983 | −0·01320 | −0·01917 |
| 0·5 | 0·56 | −0·03544 | −0·01657 | −0·02234 |
| 0·7 | 0·54 | −0·04681 | −0·02412 | −0·02580 |
| 0·75 | 0·53 | −0·05175 | −0·02771 | −0·02681 |
| 0·8 | 0·53 | −0·05453 | −0·02952 | −0·02955 |
| 0·82 | 0·53 | −0·05573 | −0·03032 | −0·02436 |
| 0·84 | 0·53 | −0·05698 | −0·03116 | −0·01499 |
| 0·86 | 0·53 | −0·05830 | −0·03205 | −0·00048 |

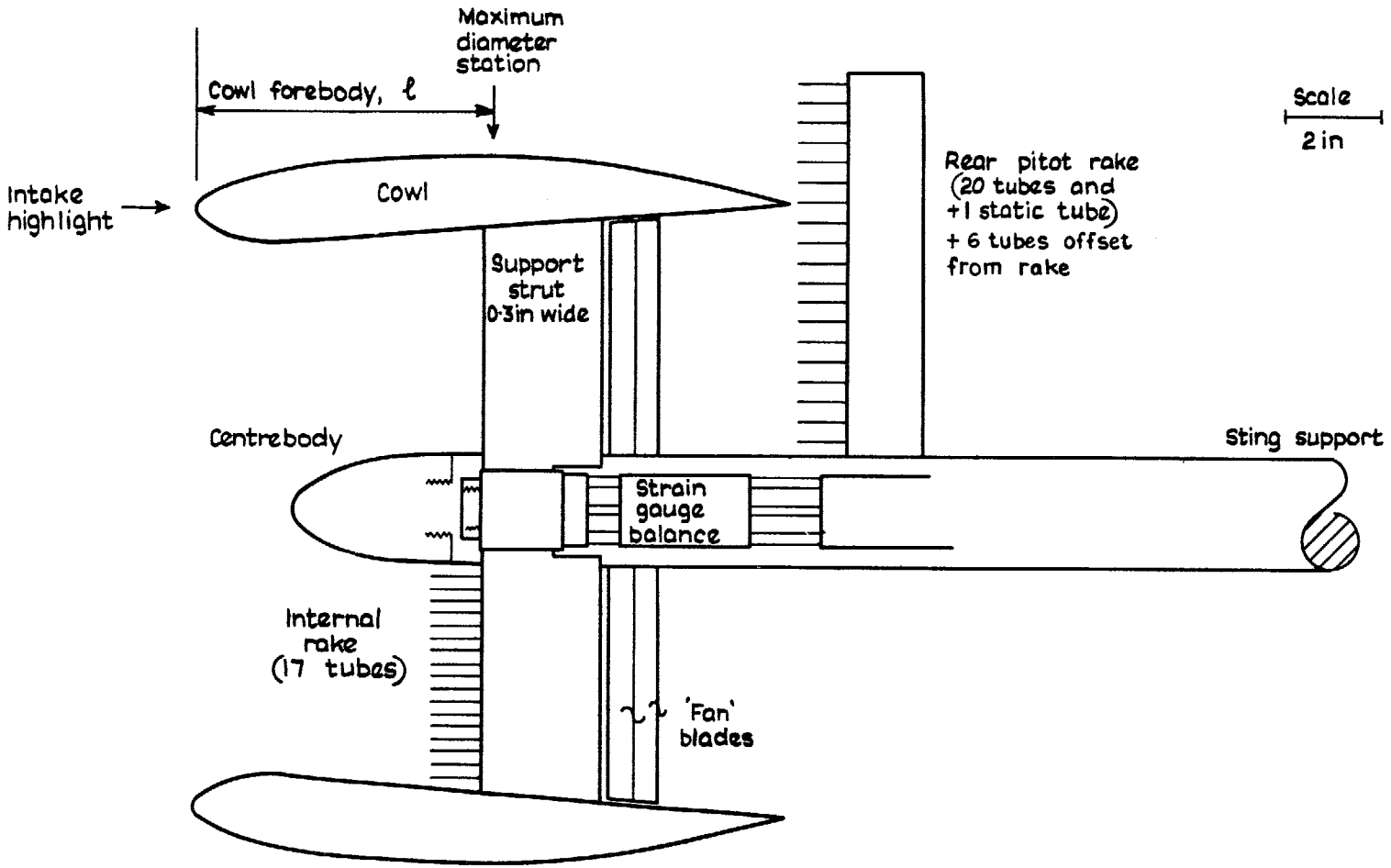


FIG. 1. Diagram of cowl rig.

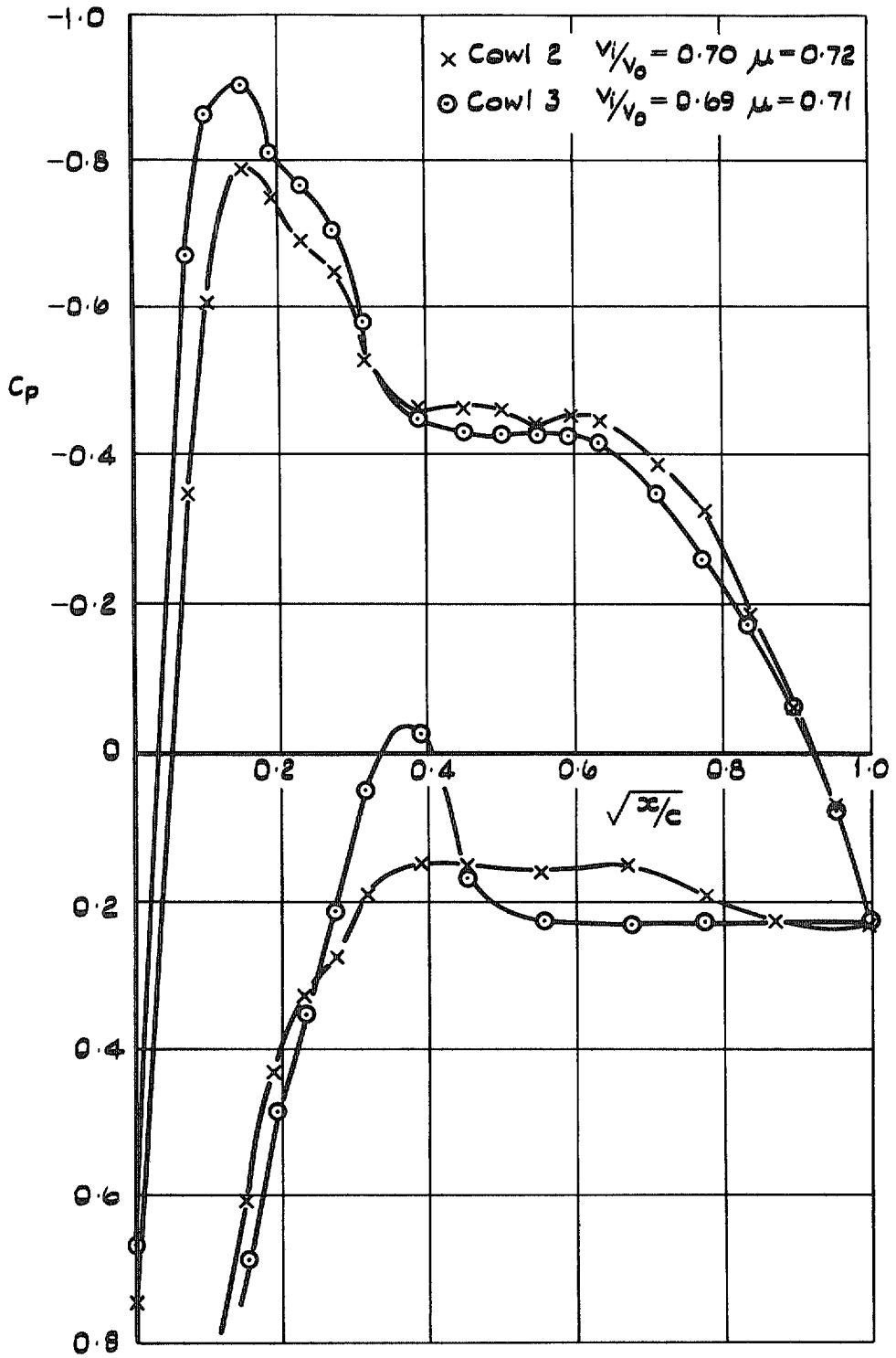


FIG. 2. Comparison between the pressure distribution on cowl 2 and cowl 3: $M = 0{\cdot}30$.

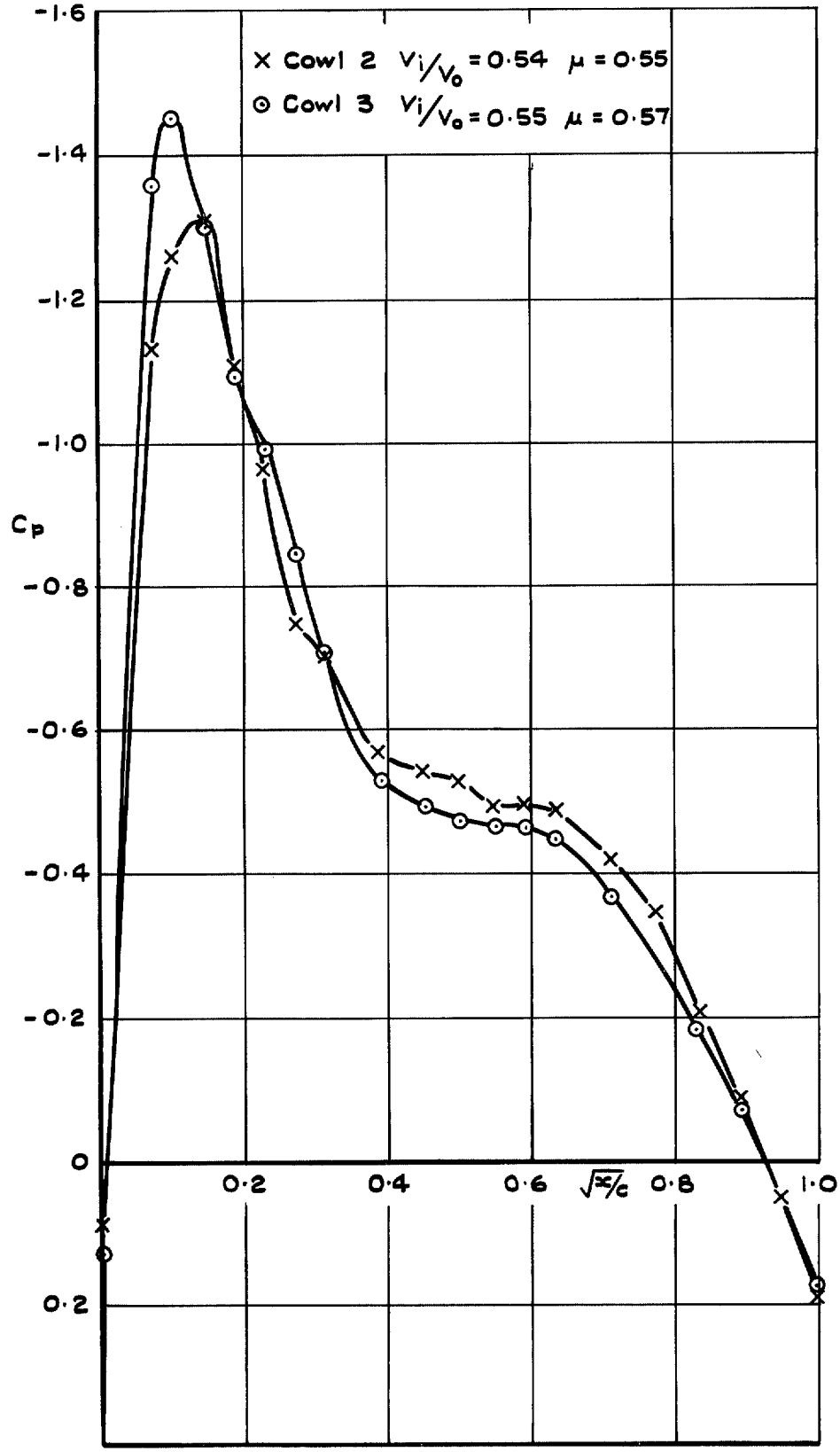


FIG. 3. Comparison between the pressure distribution on cowl 2 and cowl 3: $M = 0{\cdot}30$.

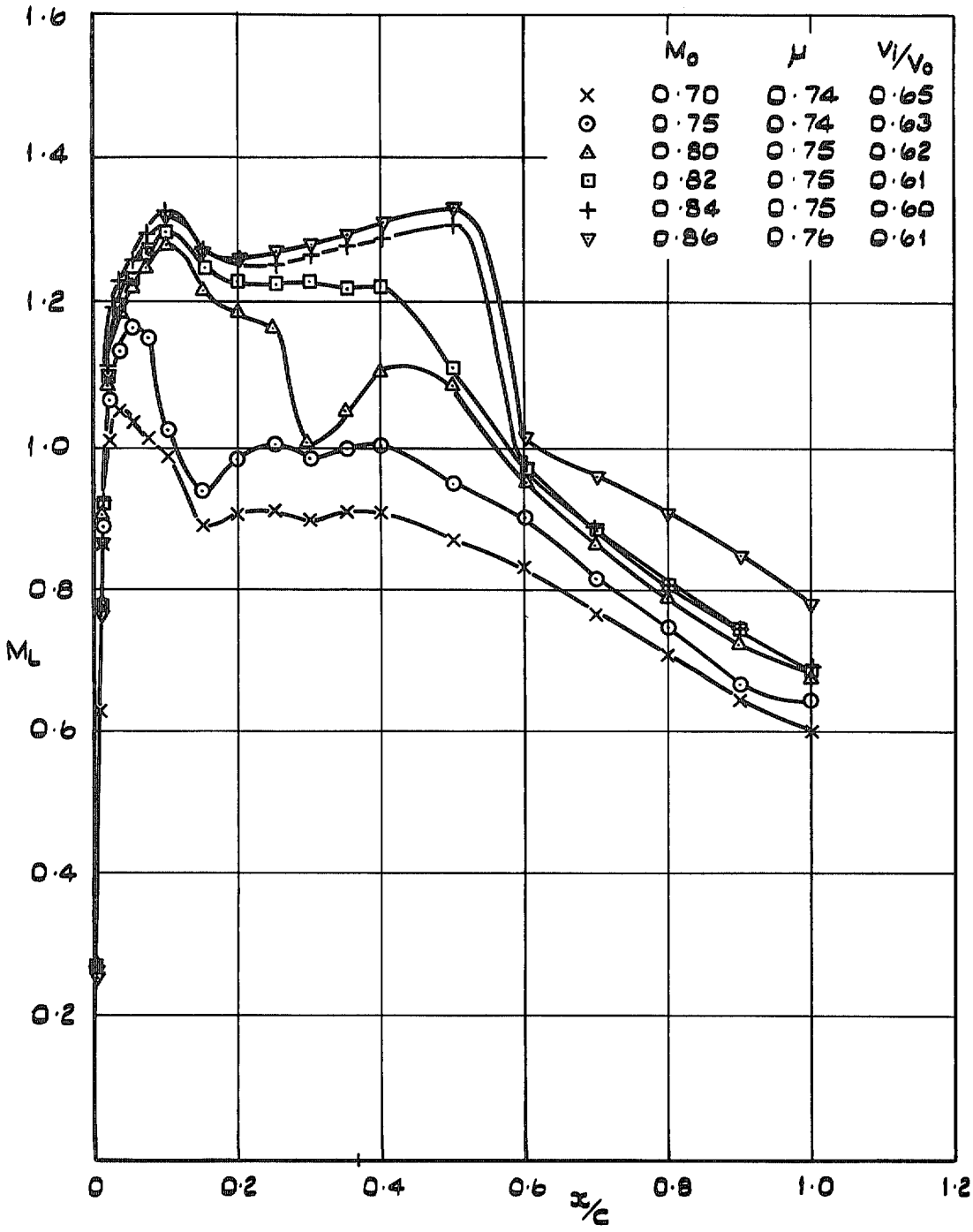


FIG. 4. Cowl 2: outer surface Mach number distribution.

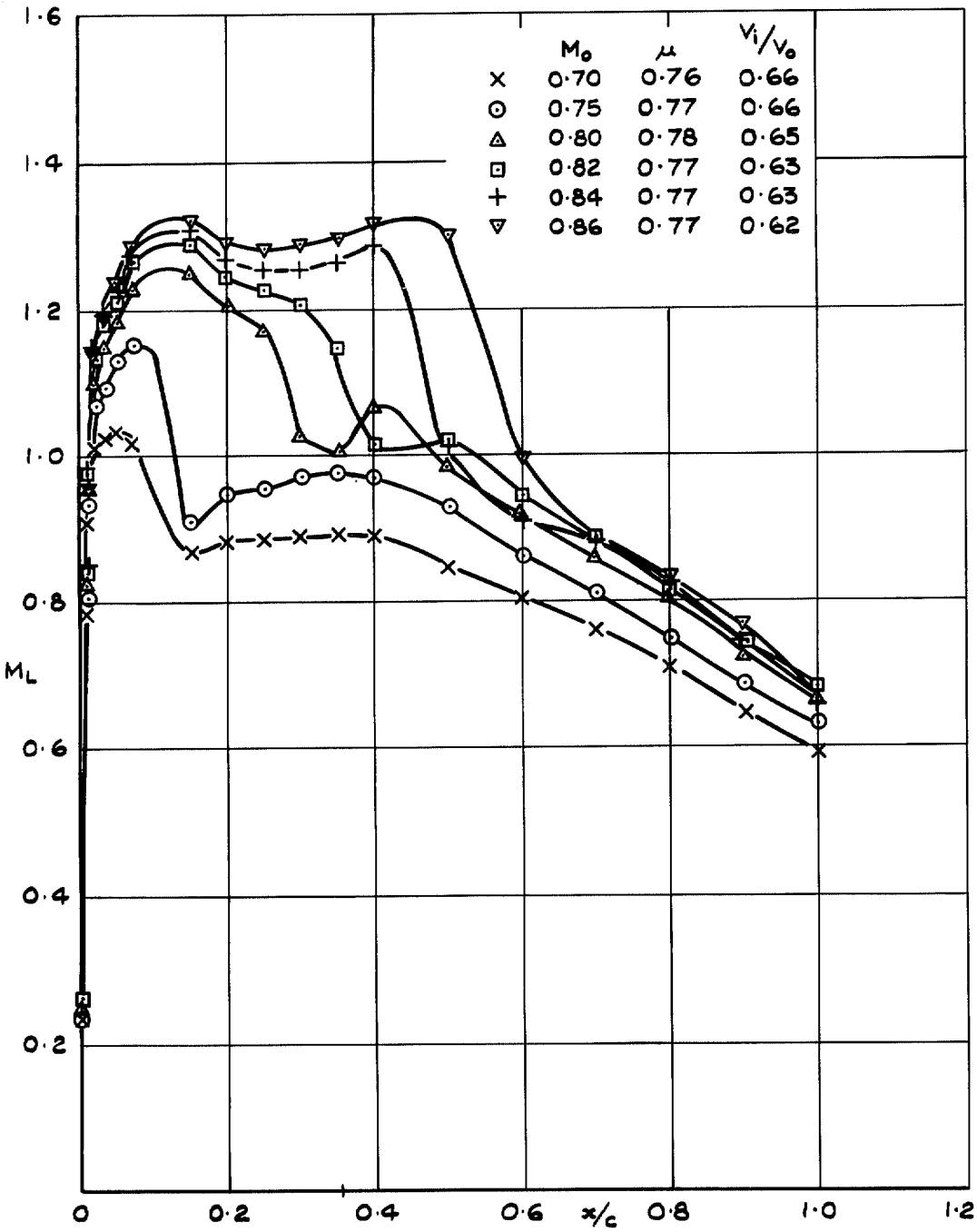


FIG. 5. Cowl 3: outer surface Mach number distribution.

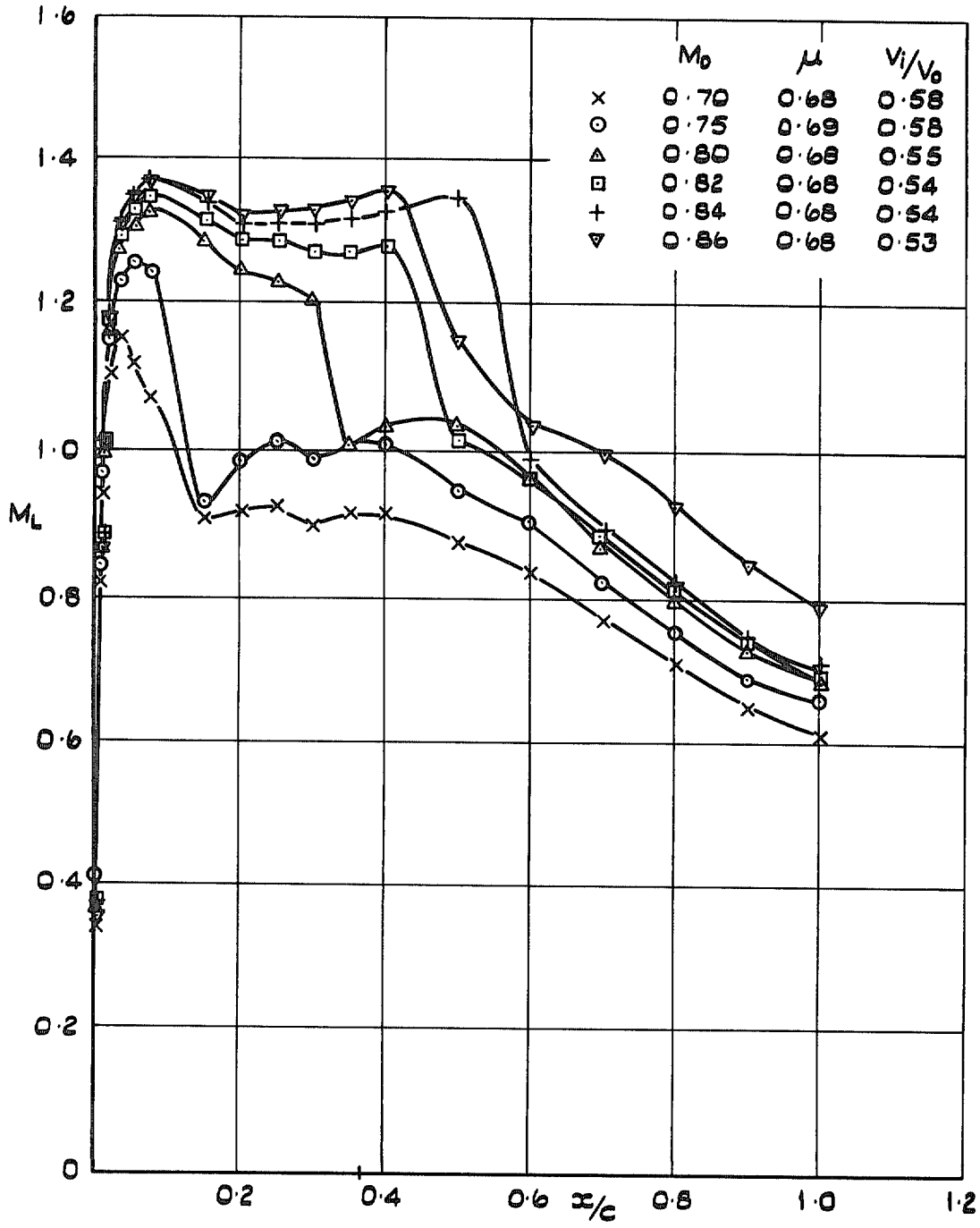


FIG. 6. Cowl 2: outer surface Mach number distribution.

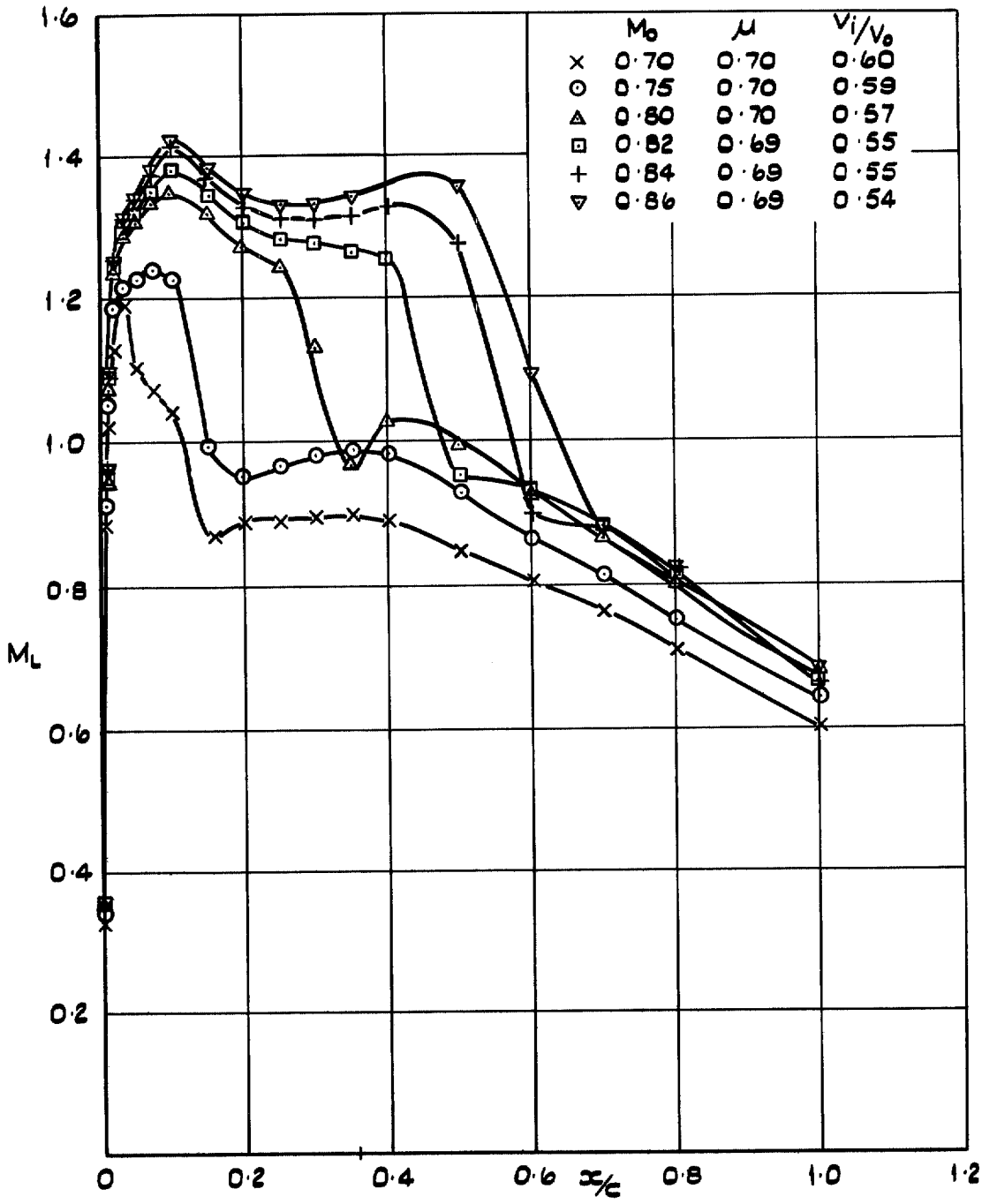


FIG. 7. Cowl 3: outer surface Mach number distribution.

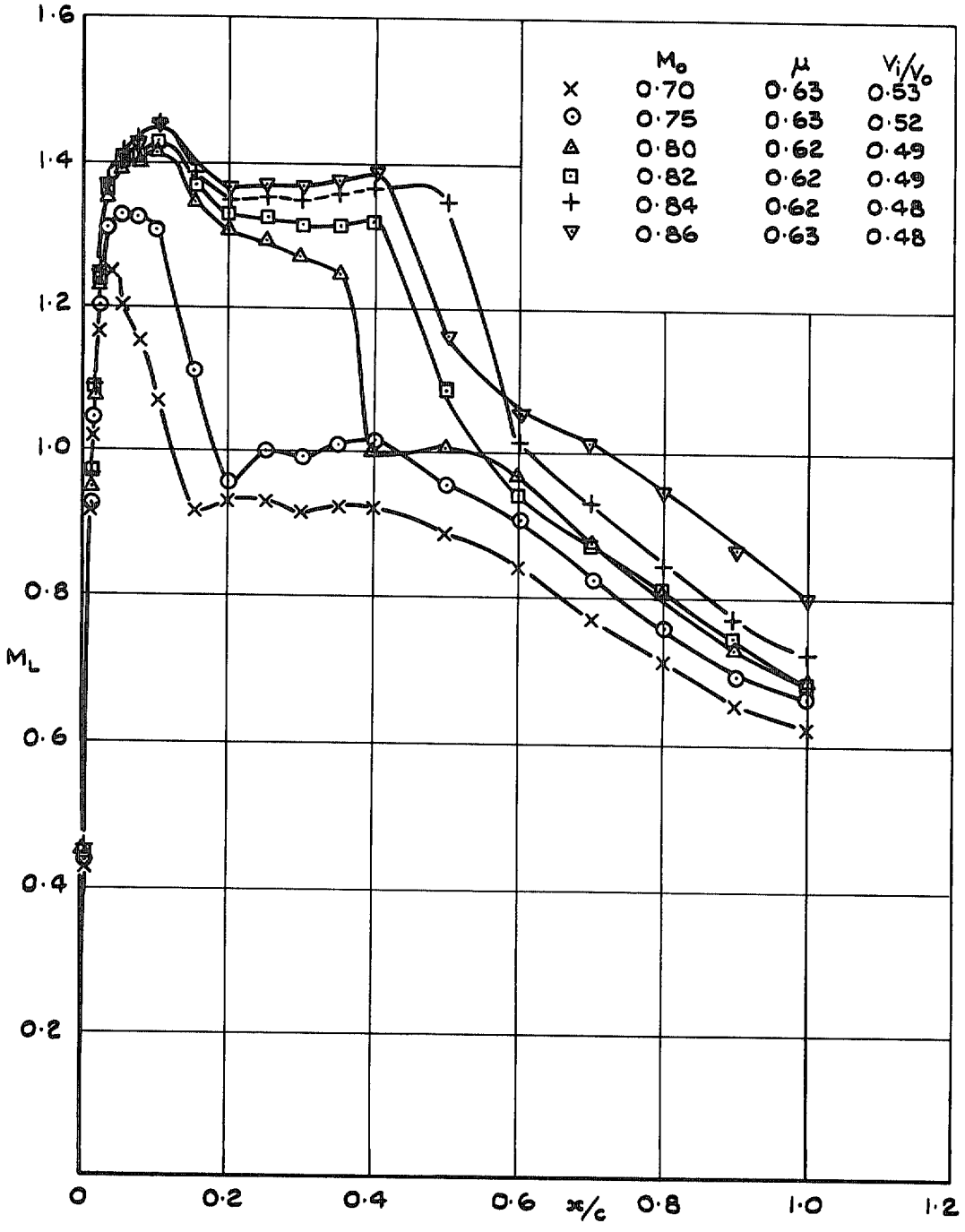


FIG. 8. Cowl 2: outer surface Mach number distribution.

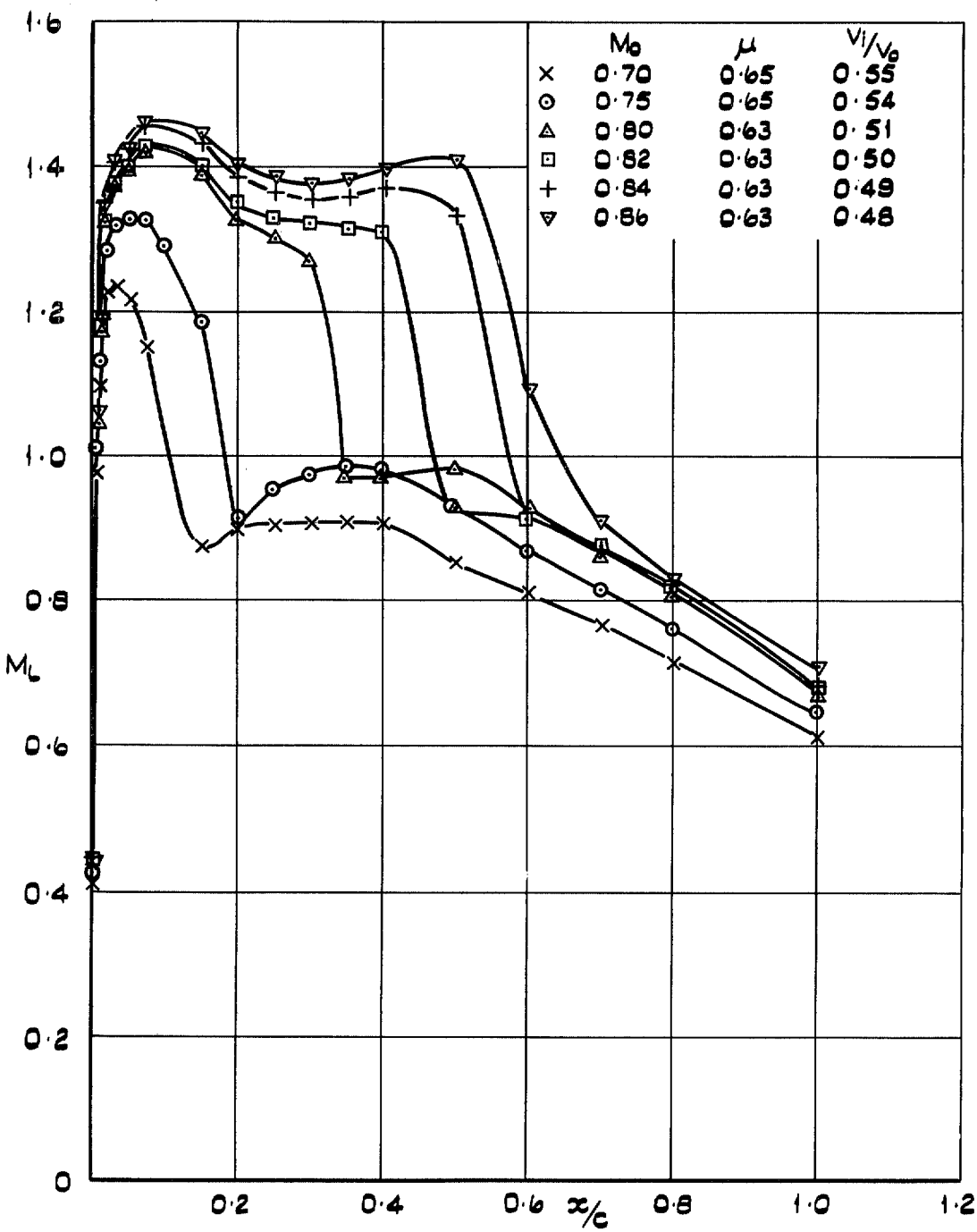


FIG. 9. Cowl 3: outer surface Mach number distribution.

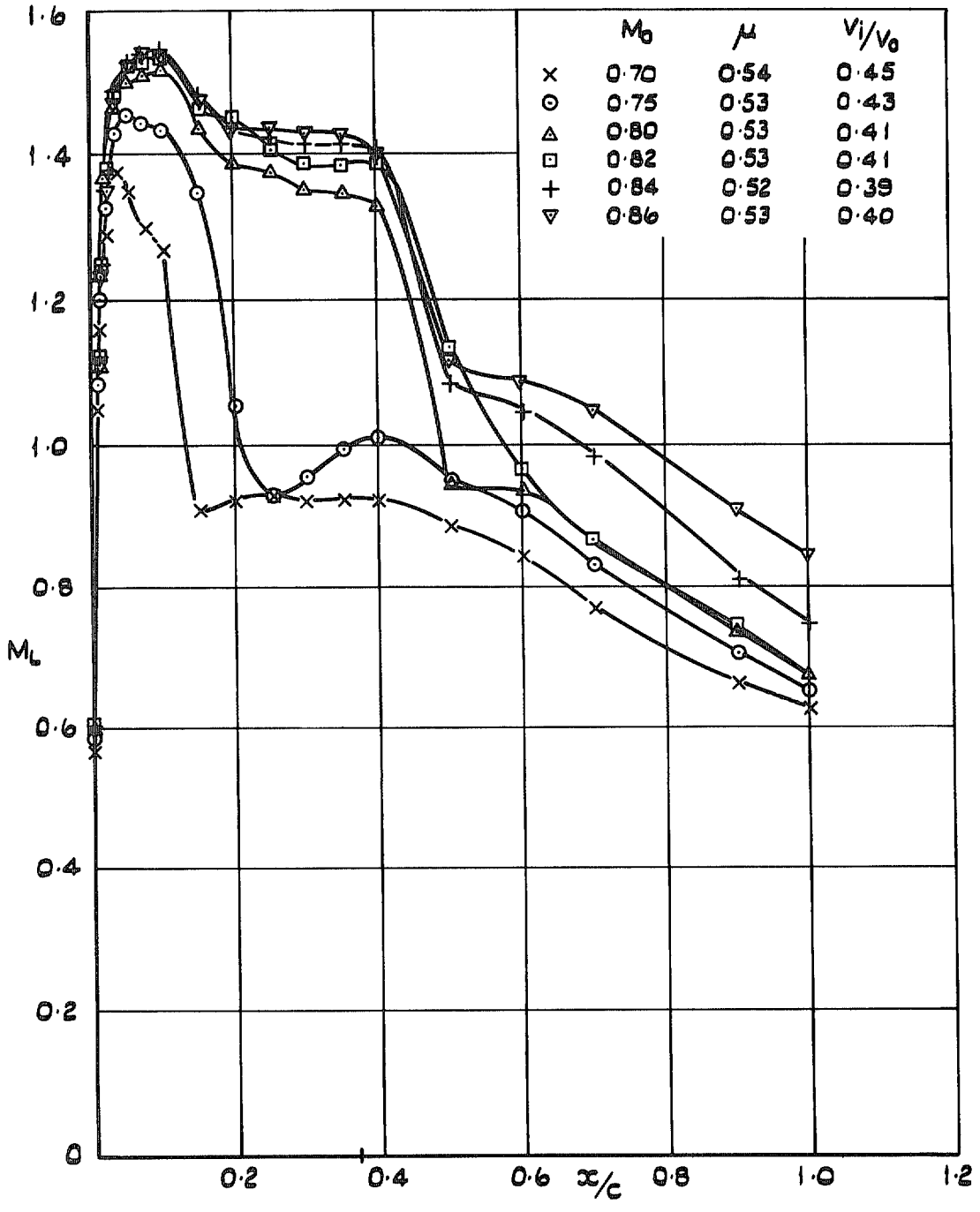


FIG. 10. Cowl 2: outer surface Mach number distribution.

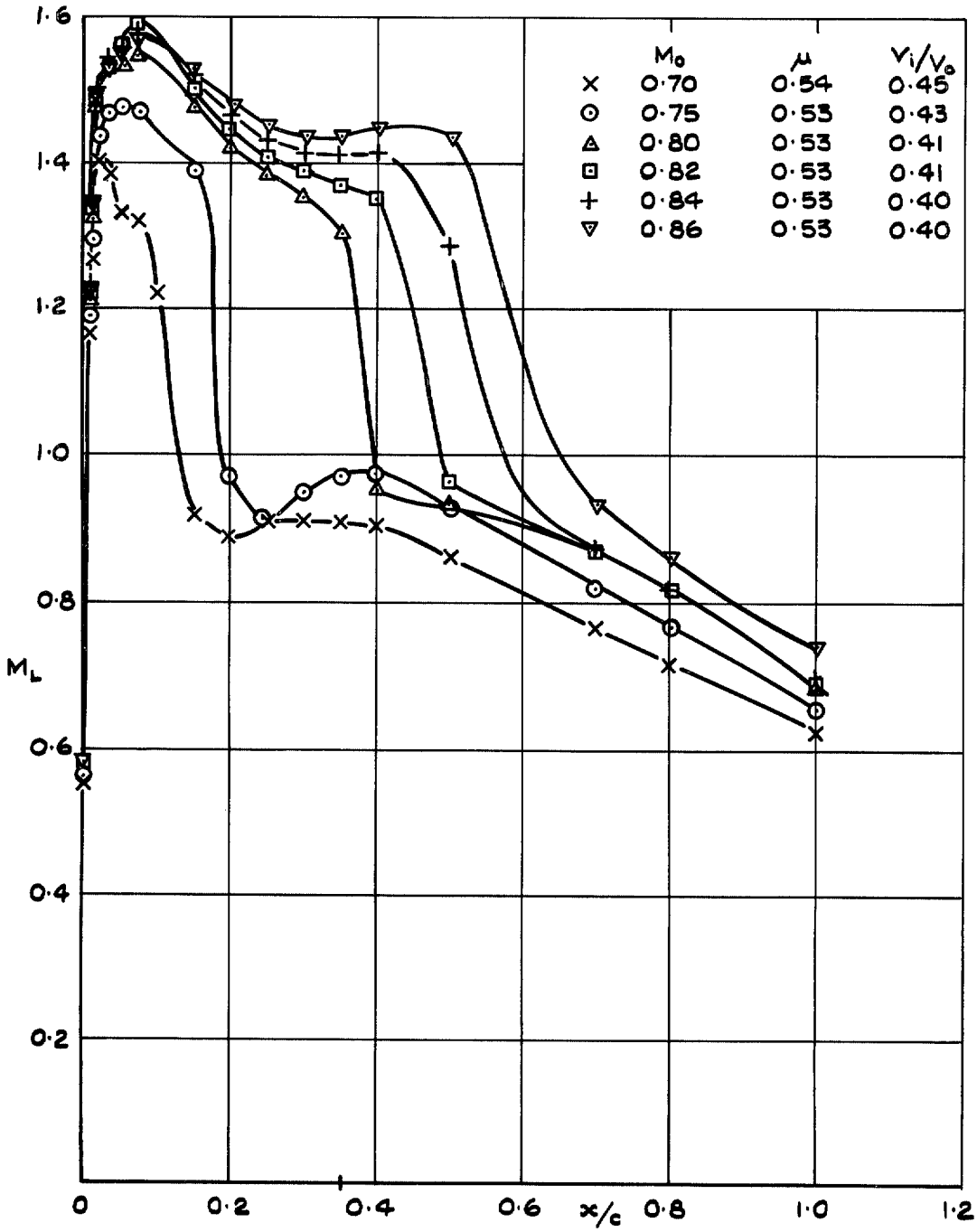


FIG. 11. Cowl 3: outer surface Mach number distribution.

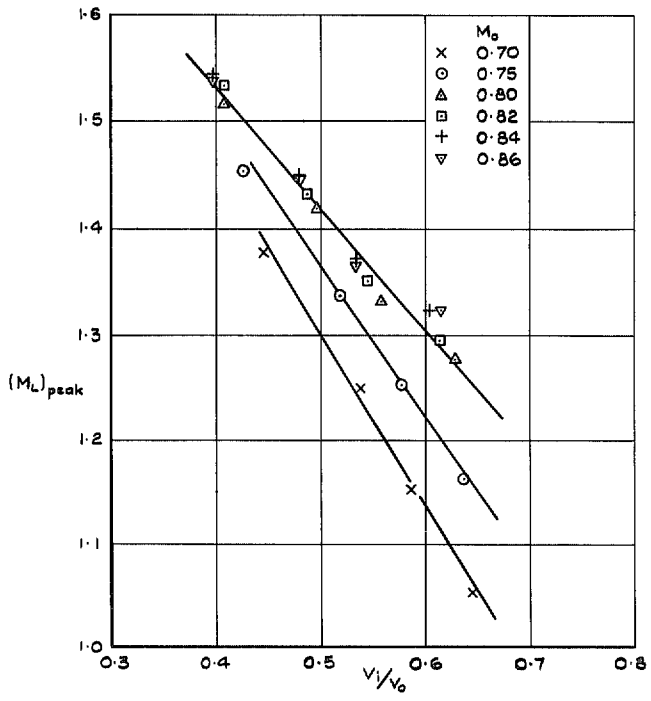


FIG. 12. Peak Mach number on cowl 2 outer surface $v$ velocity ratio.

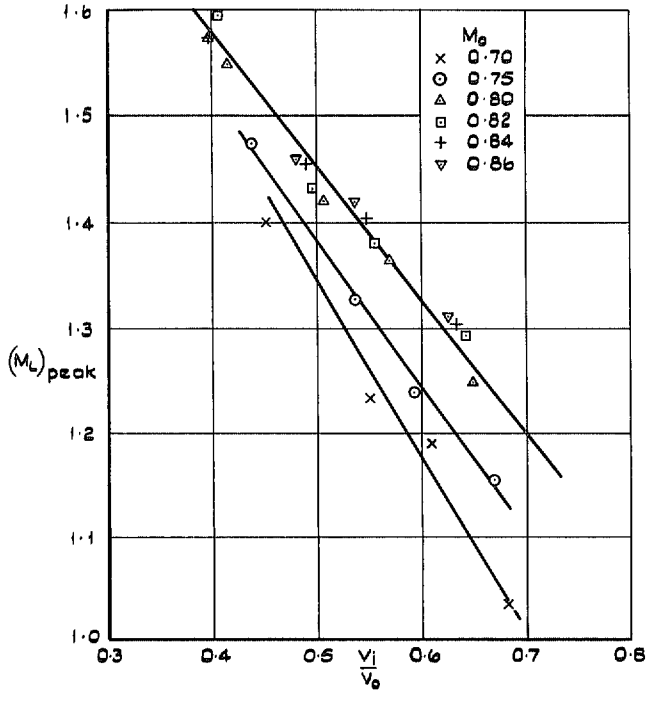


FIG. 13. Peak Mach number on cowl 3 outer surface $v$ velocity ratio.

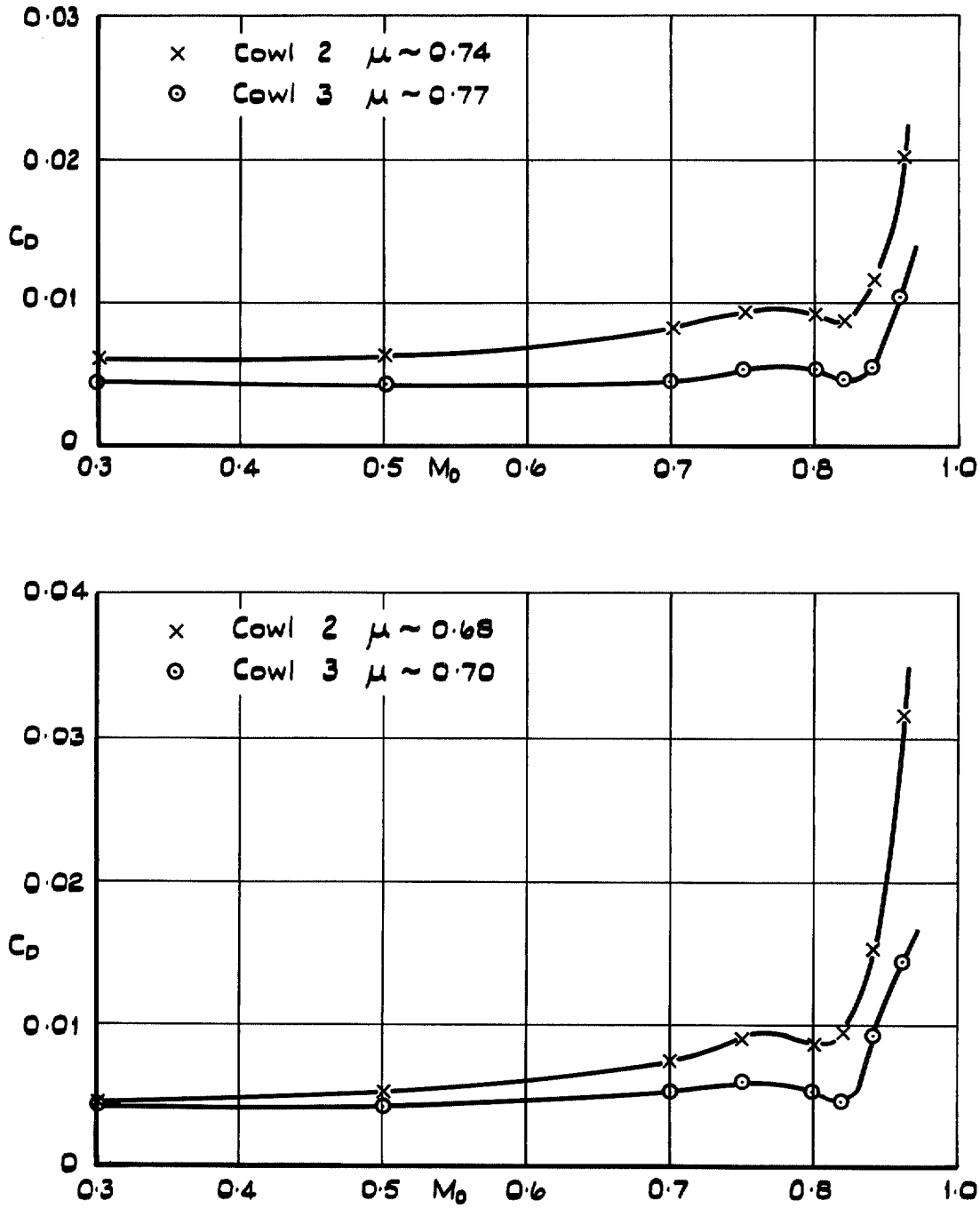


FIG. 14. Drag coefficients based on reference area $2\pi r_i c$.

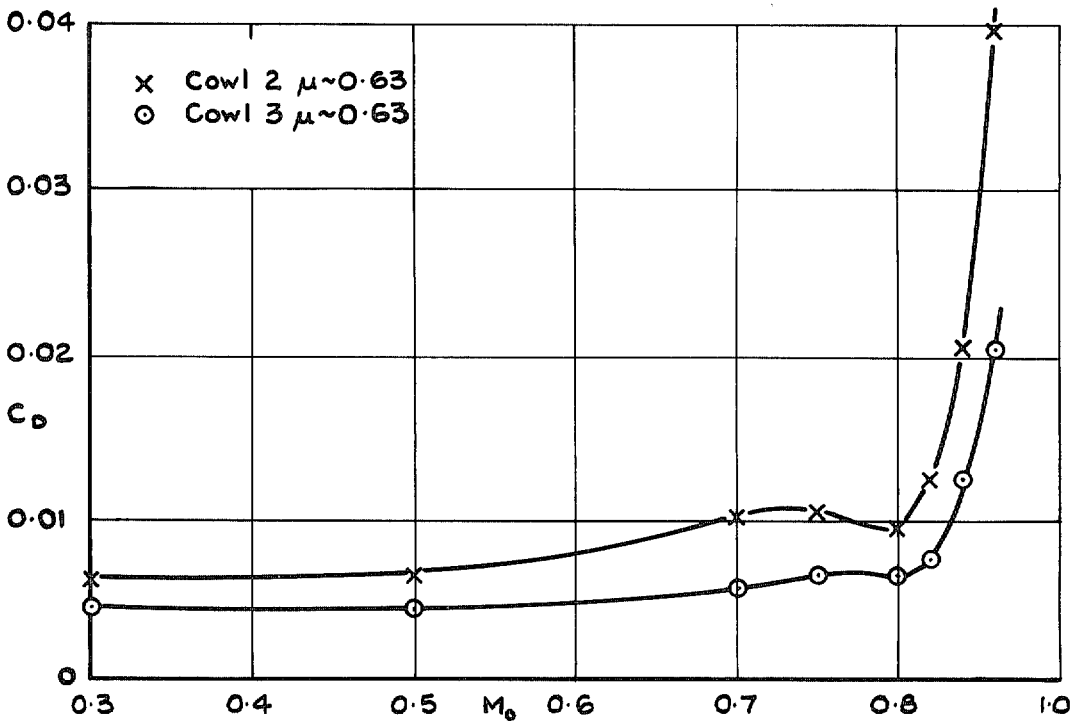


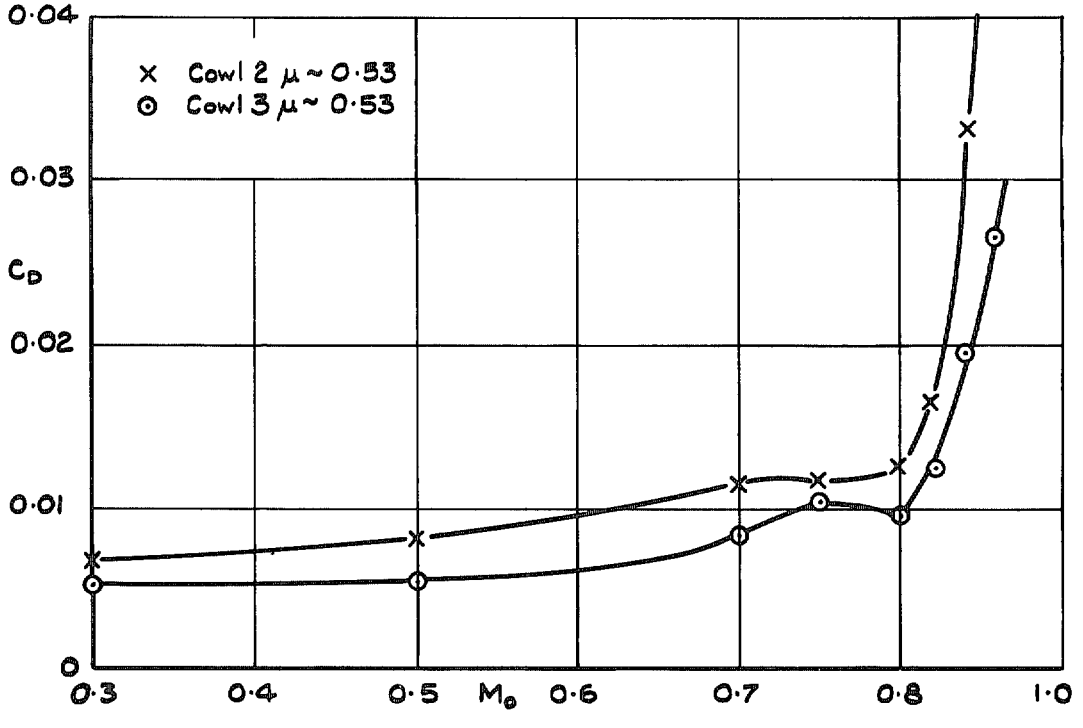


FIG. 15. Drag coefficients based on reference area $2\pi r_i c$.

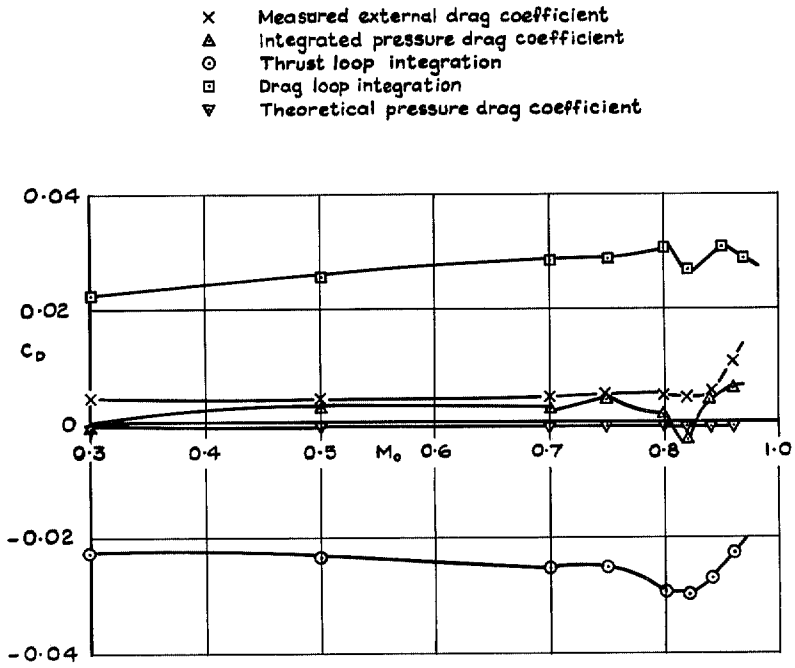


FIG. 16. Drag components: cowl 3: $\mu \sim 0{\cdot}77$.

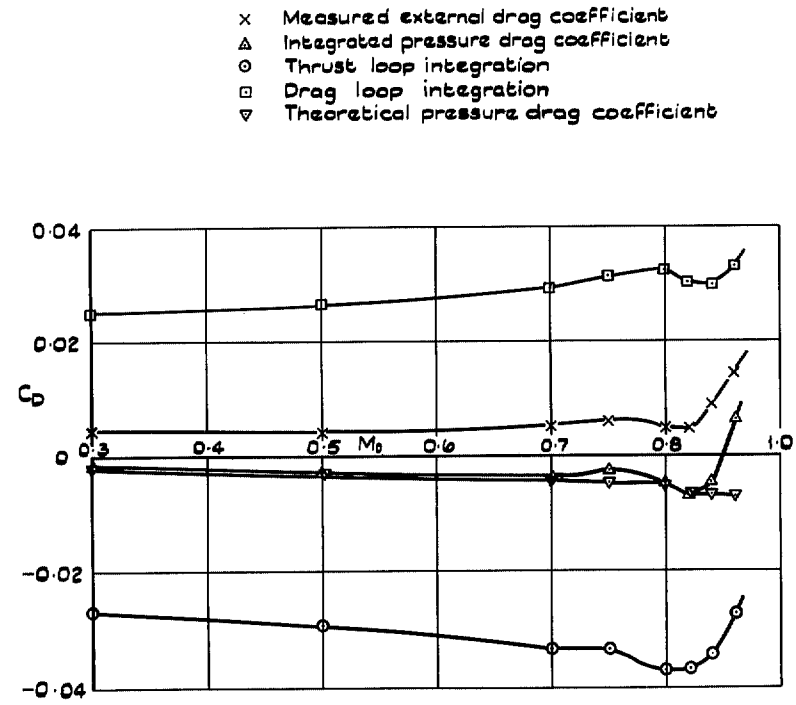


FIG. 17. Drag components: cowl 3: $\mu \sim 0{\cdot}70$.

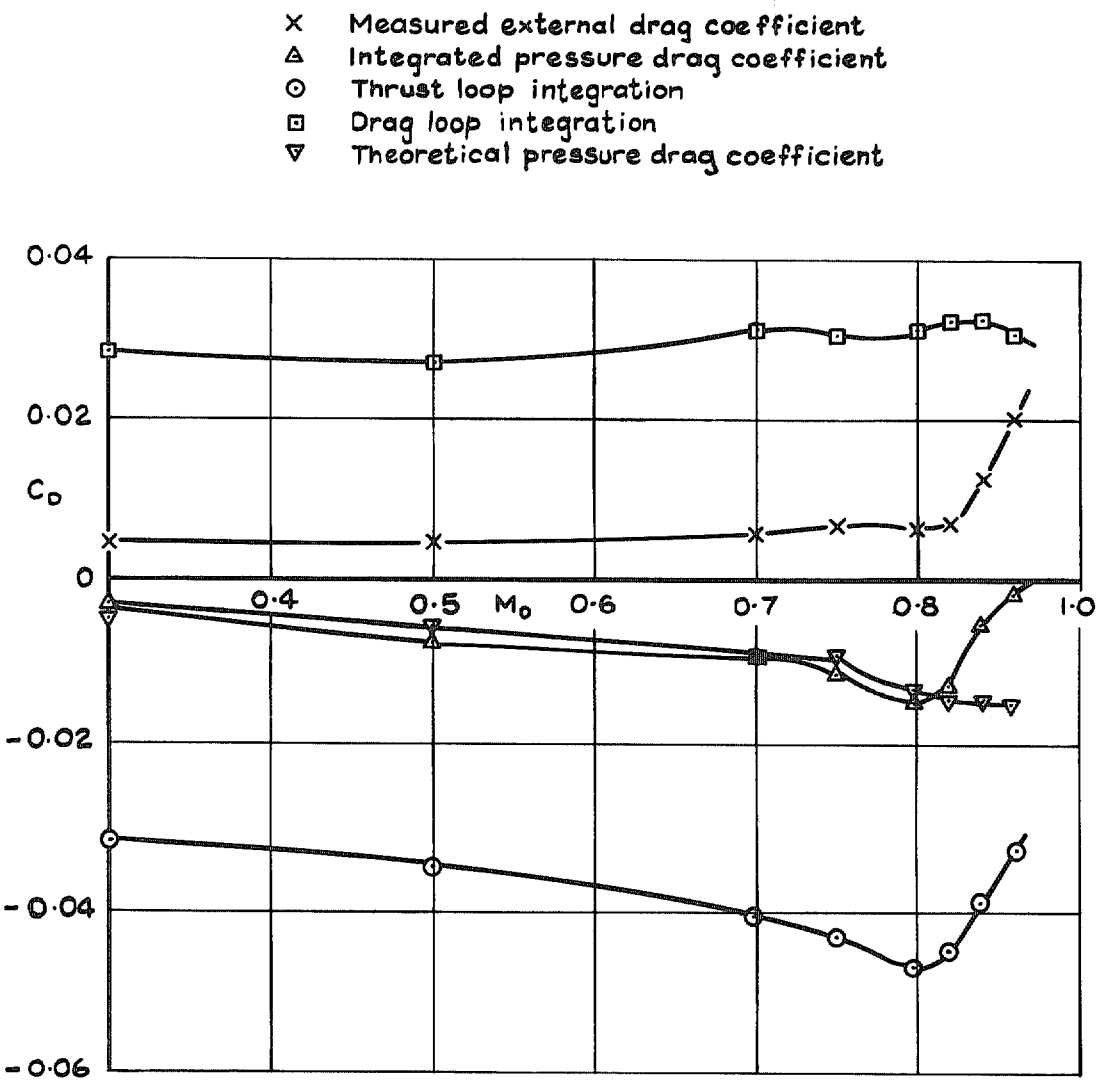


FIG. 18. Drag components: cowl 3: $\mu \sim 0{\cdot}63$.

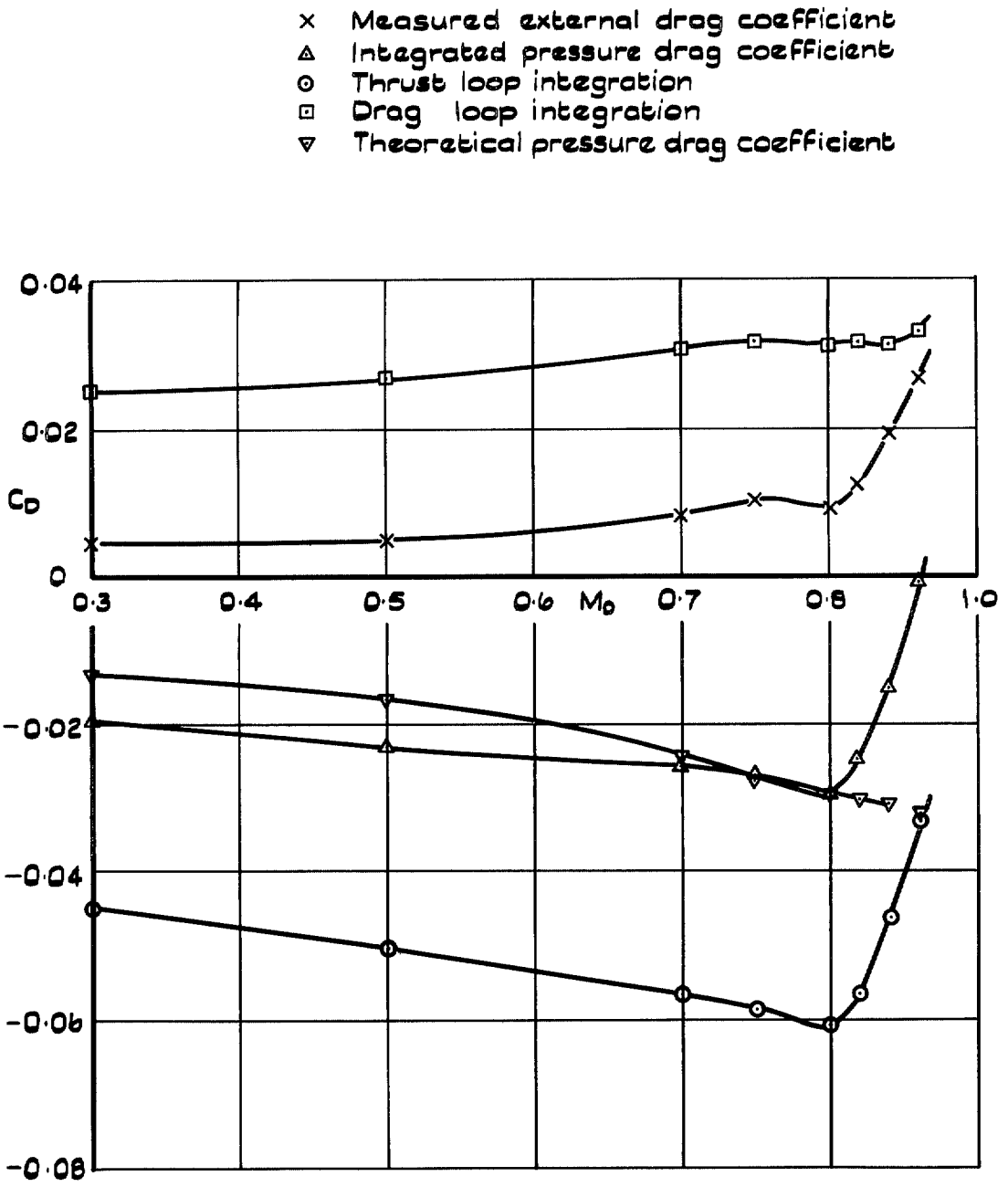


FIG. 19. Drag components: cowl 3: $\mu \sim 0{\cdot}53$.

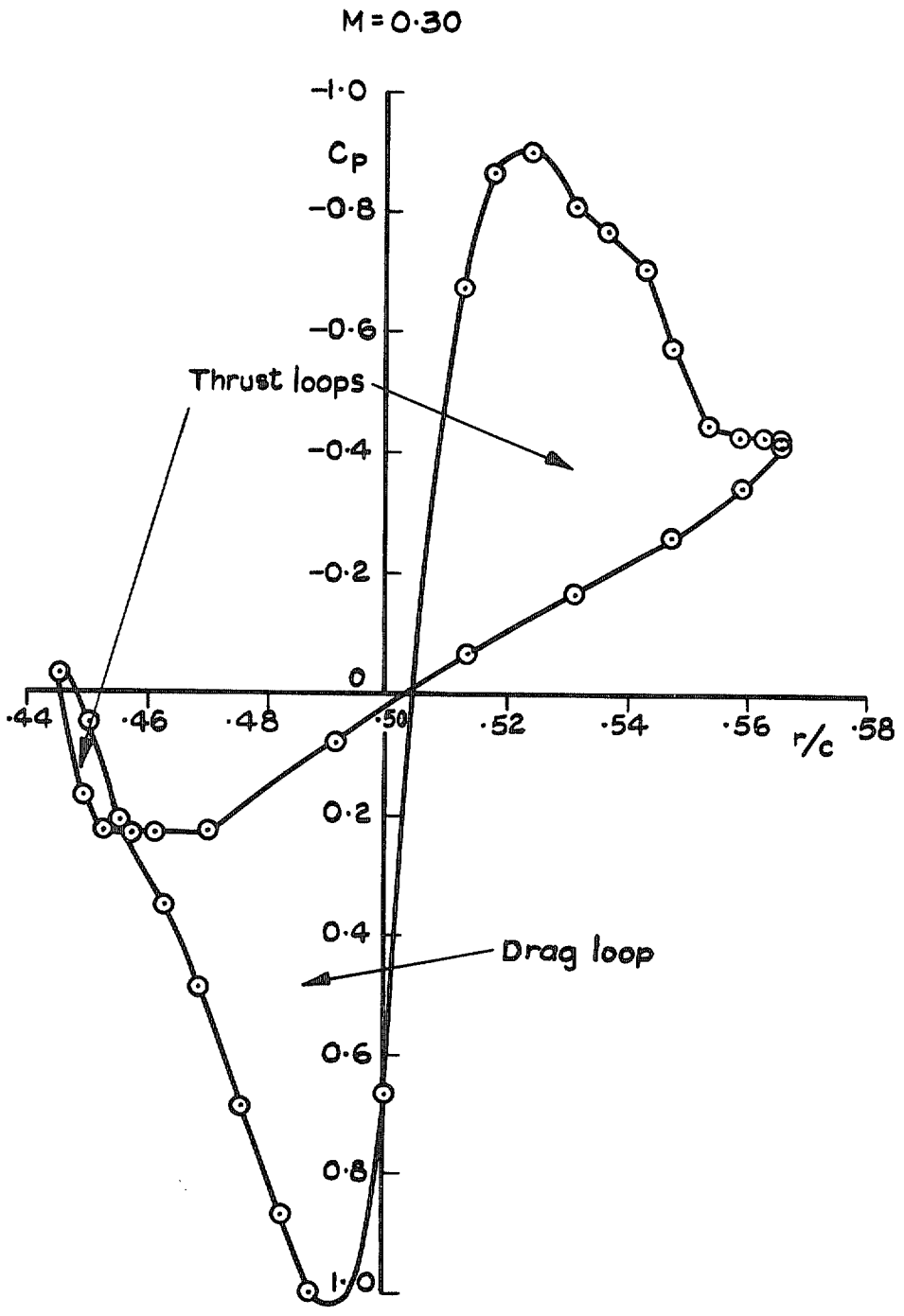


FIG. 20. Thrust and drag loops: cowl 3: $\mu = 0{\cdot}71$: $M = 0{\cdot}3$.

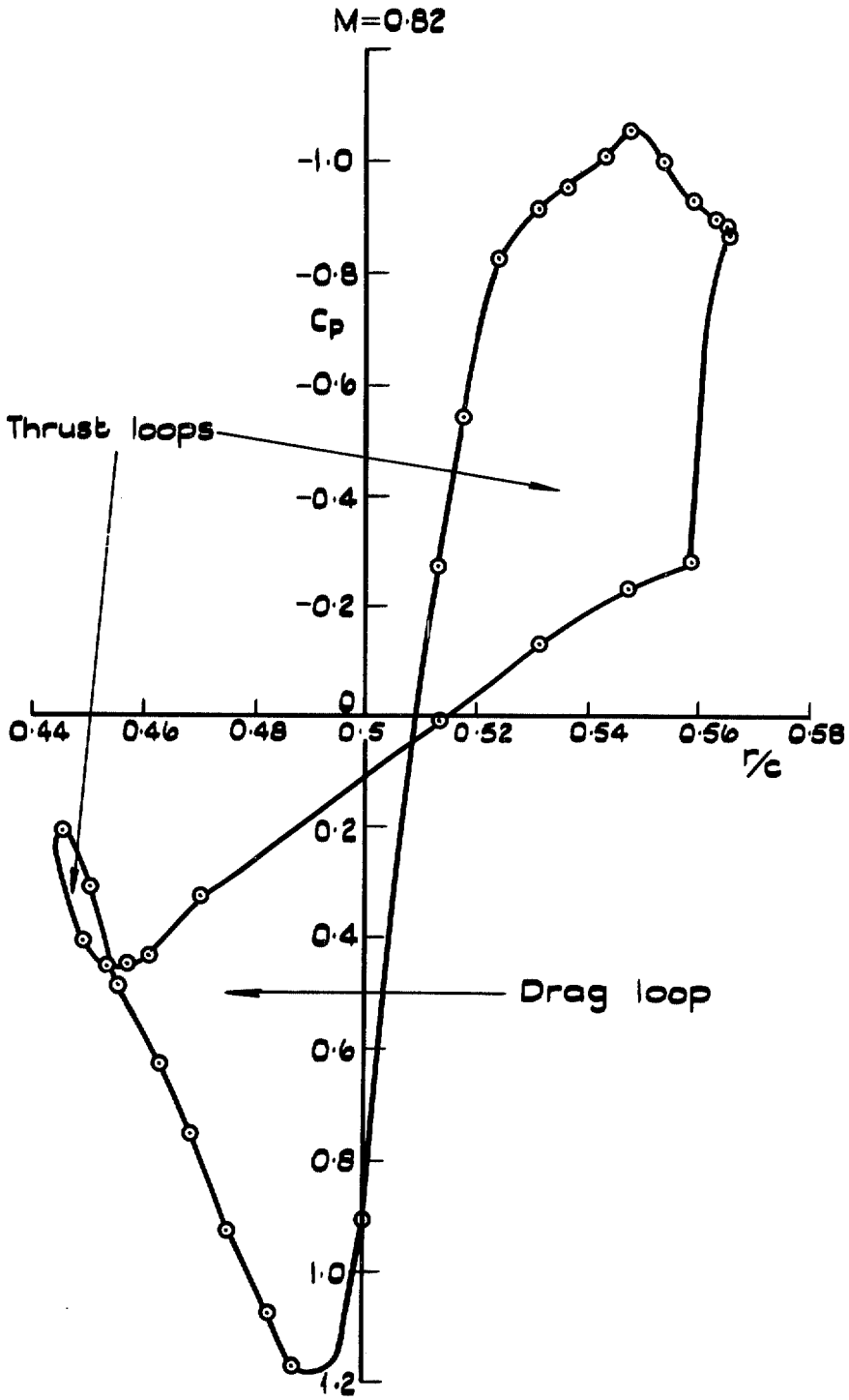


FIG. 21. Thrust and drag loops: cowl 3 : $\mu = 0{\cdot}69$ : $M = 0{\cdot}82$.

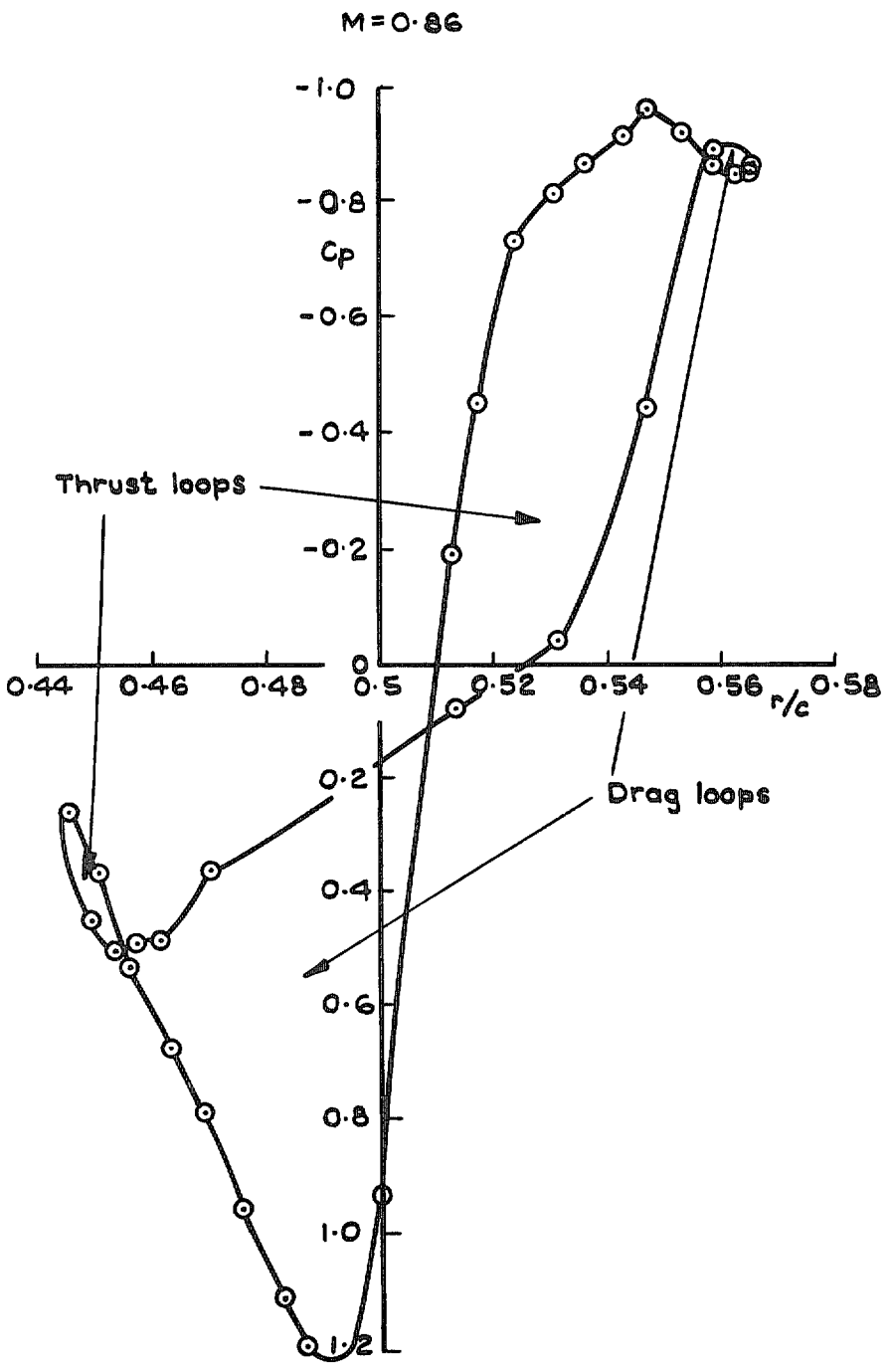


FIG. 22. Thrust and drag loops: cowl 3: $\mu = 0{\cdot}69$: $M = 0{\cdot}86$.

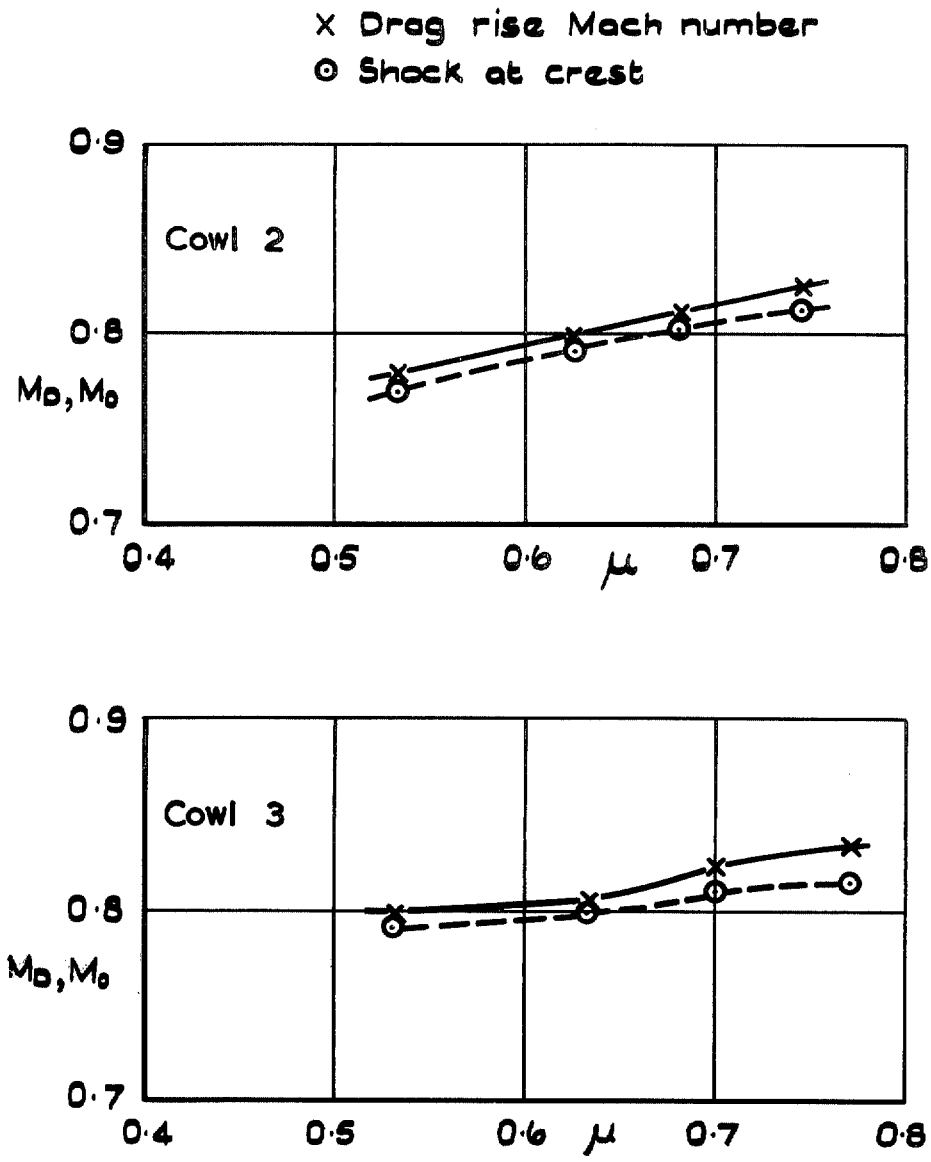


FIG. 23. Drag-rise Mach number and 'shock at crest' $v$ mass-flow ratio.

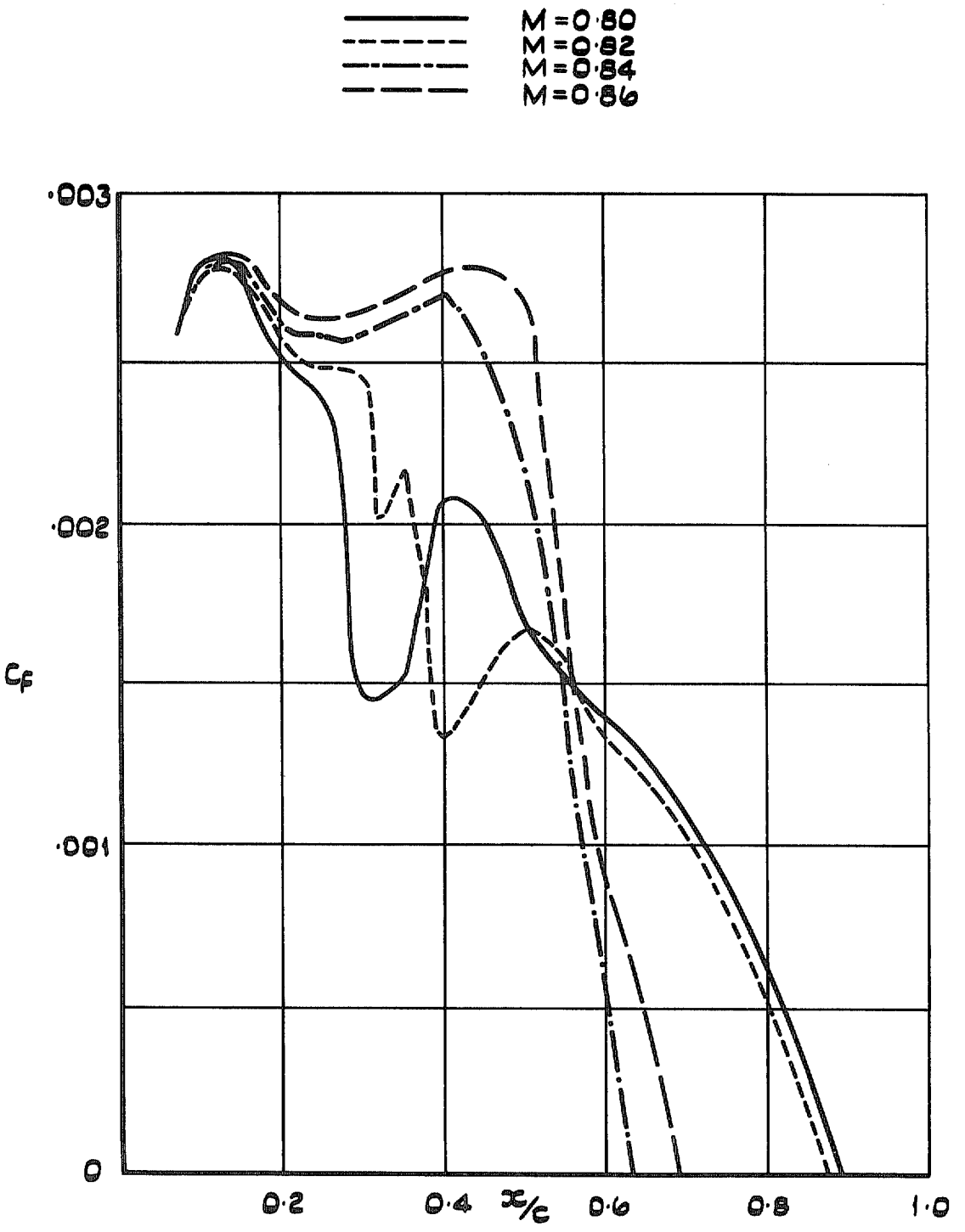


FIG. 24. Calculated skin-friction coefficients cowl 3: $\mu = 0{\cdot}77$: $M = 0{\cdot}80$–$0{\cdot}86$.

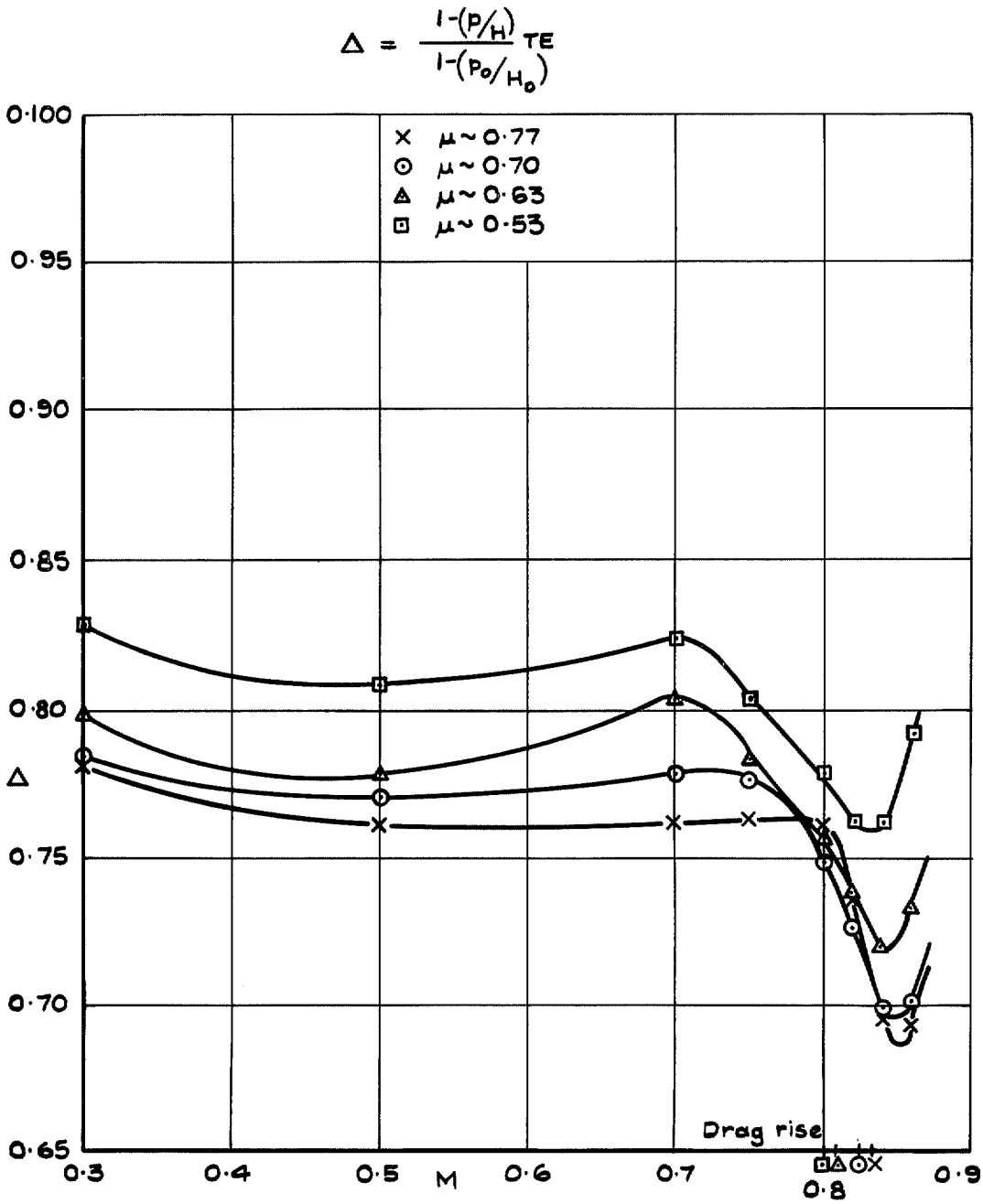


FIG. 25. Trailing-edge pressure parameter $v$ Mach number: cowl 3.

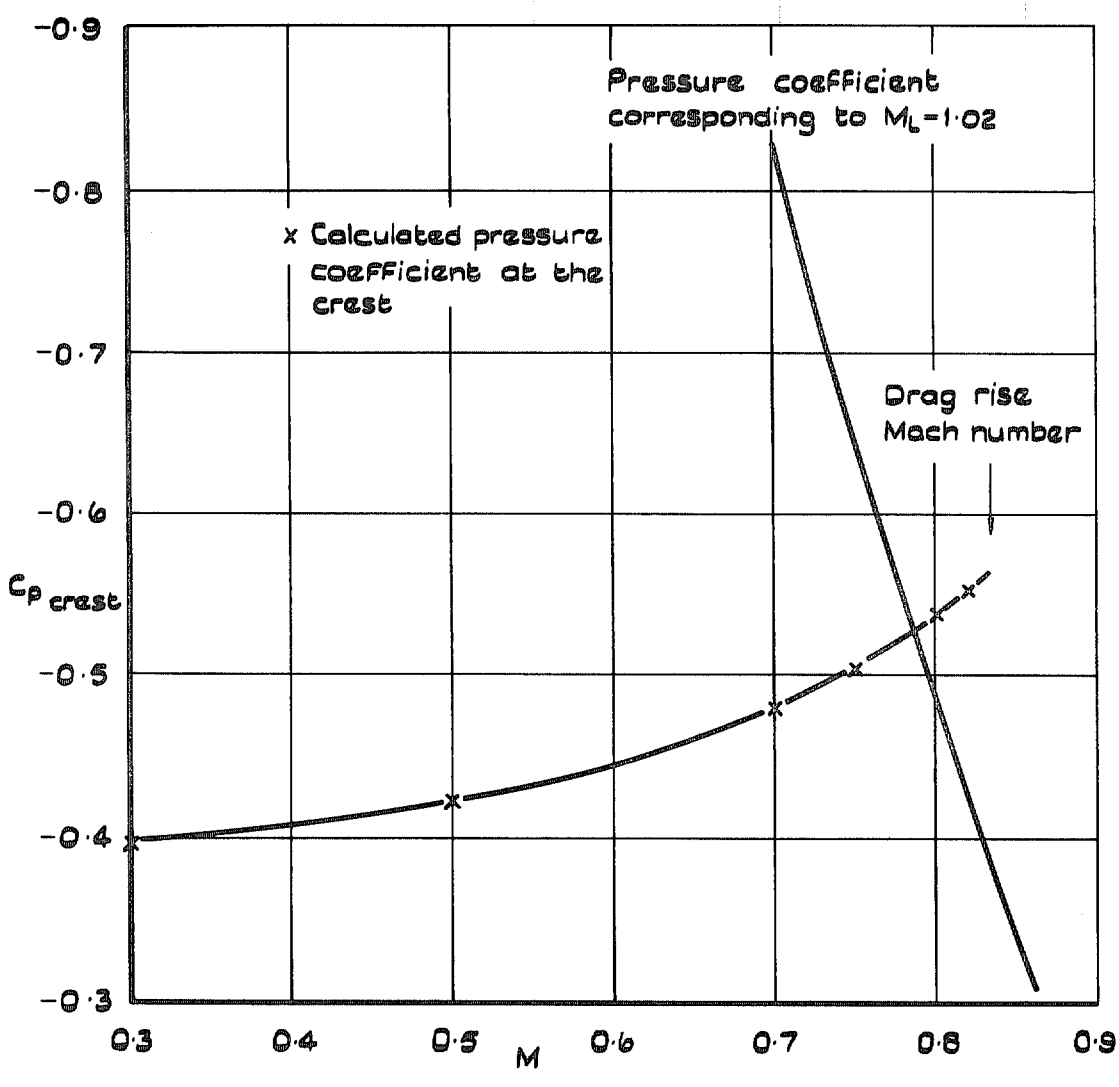


FIG. 26. Calculated pressure coefficient at the crest: cowl 3; $\mu = 0{\cdot}76$.

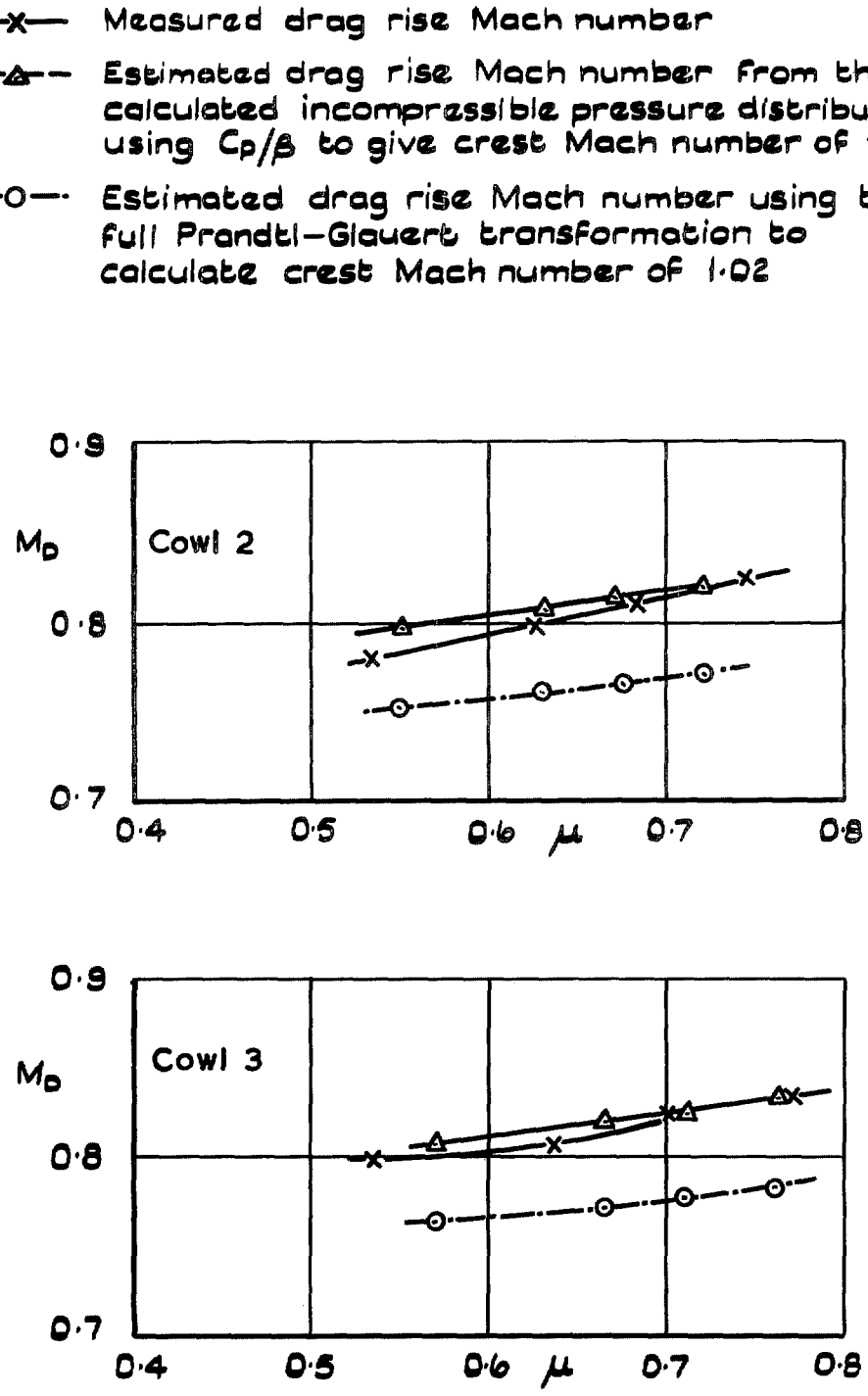


FIG. 27. Theoretical estimation of the drag-rise Mach number.

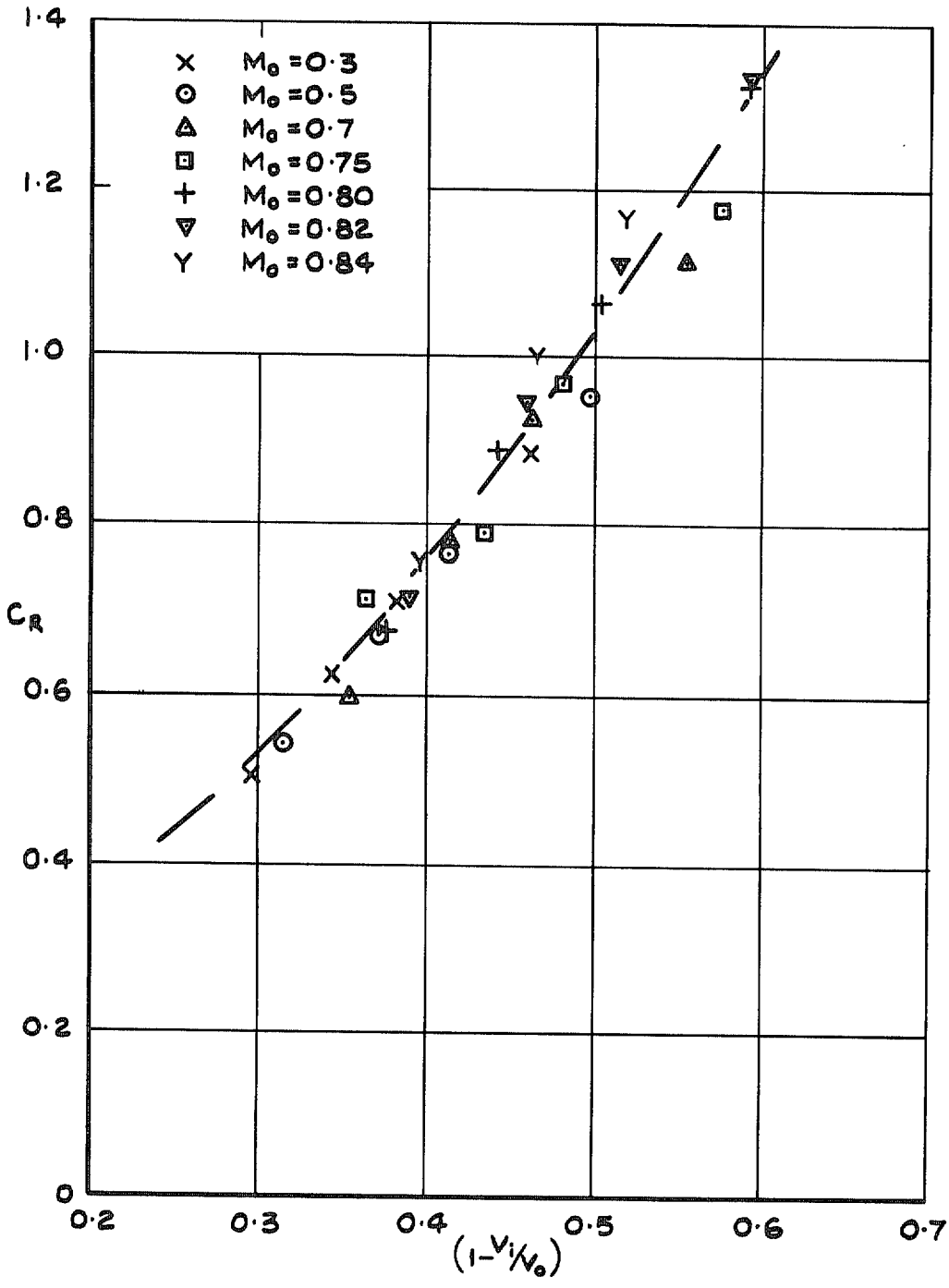


FIG. 28. Radial force coefficient $v(1 - V_i/V_0)$: cowl 2.

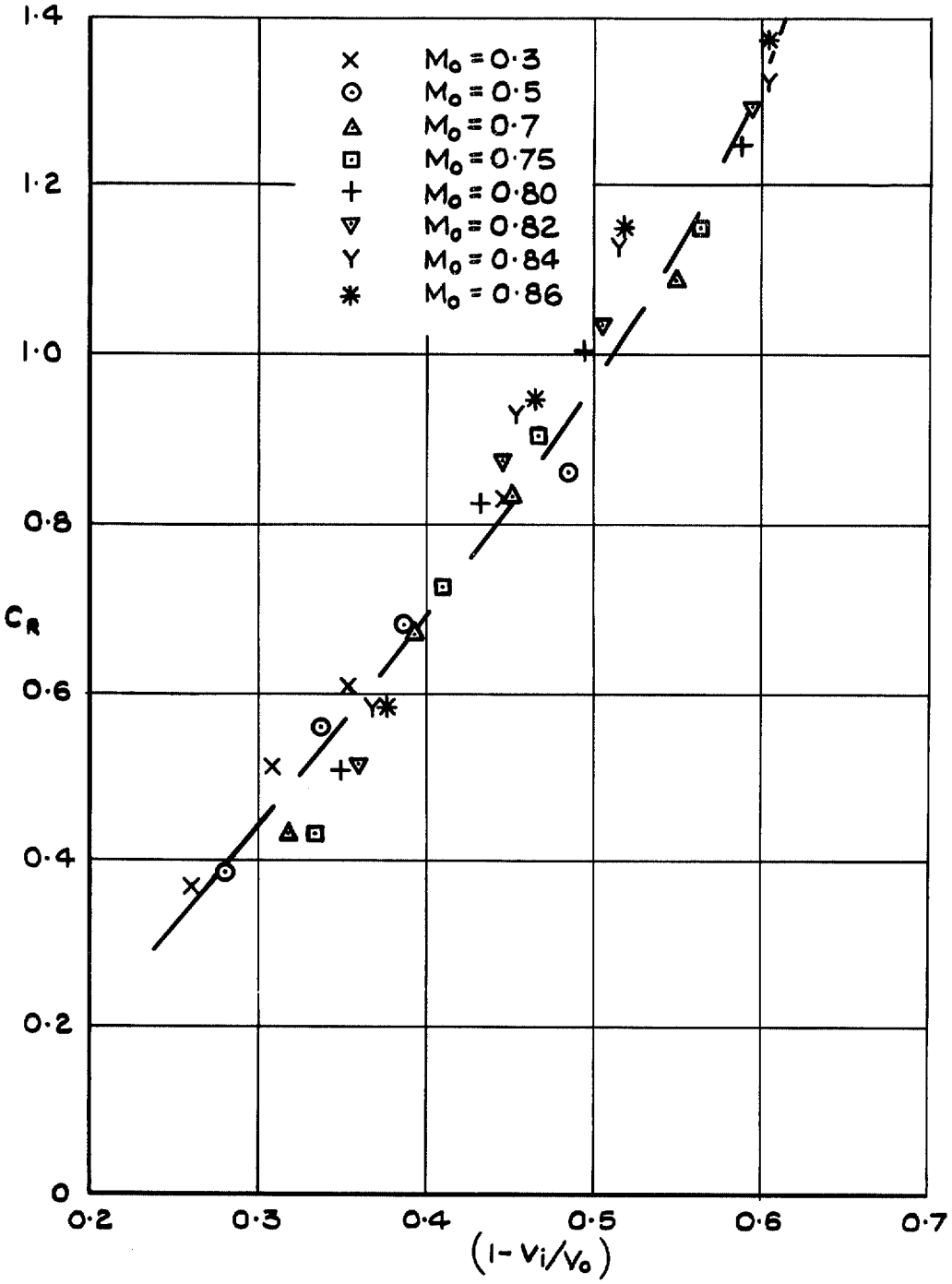


FIG. 29. Radial force coefficient $v(1 - V_i/V_0)$: cowl 3.

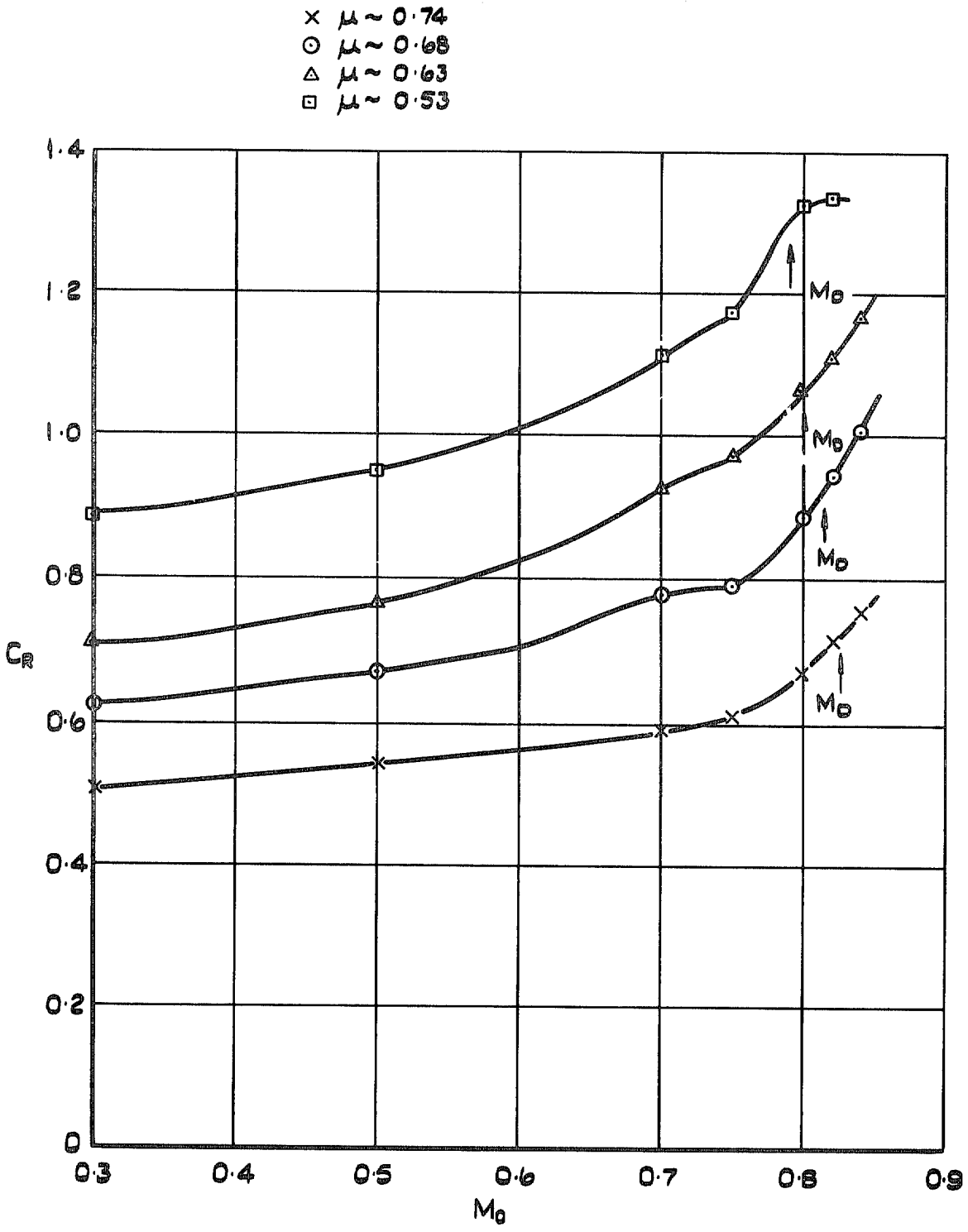


FIG. 30. Radial force coefficient $v$ Mach number: cowl 2.

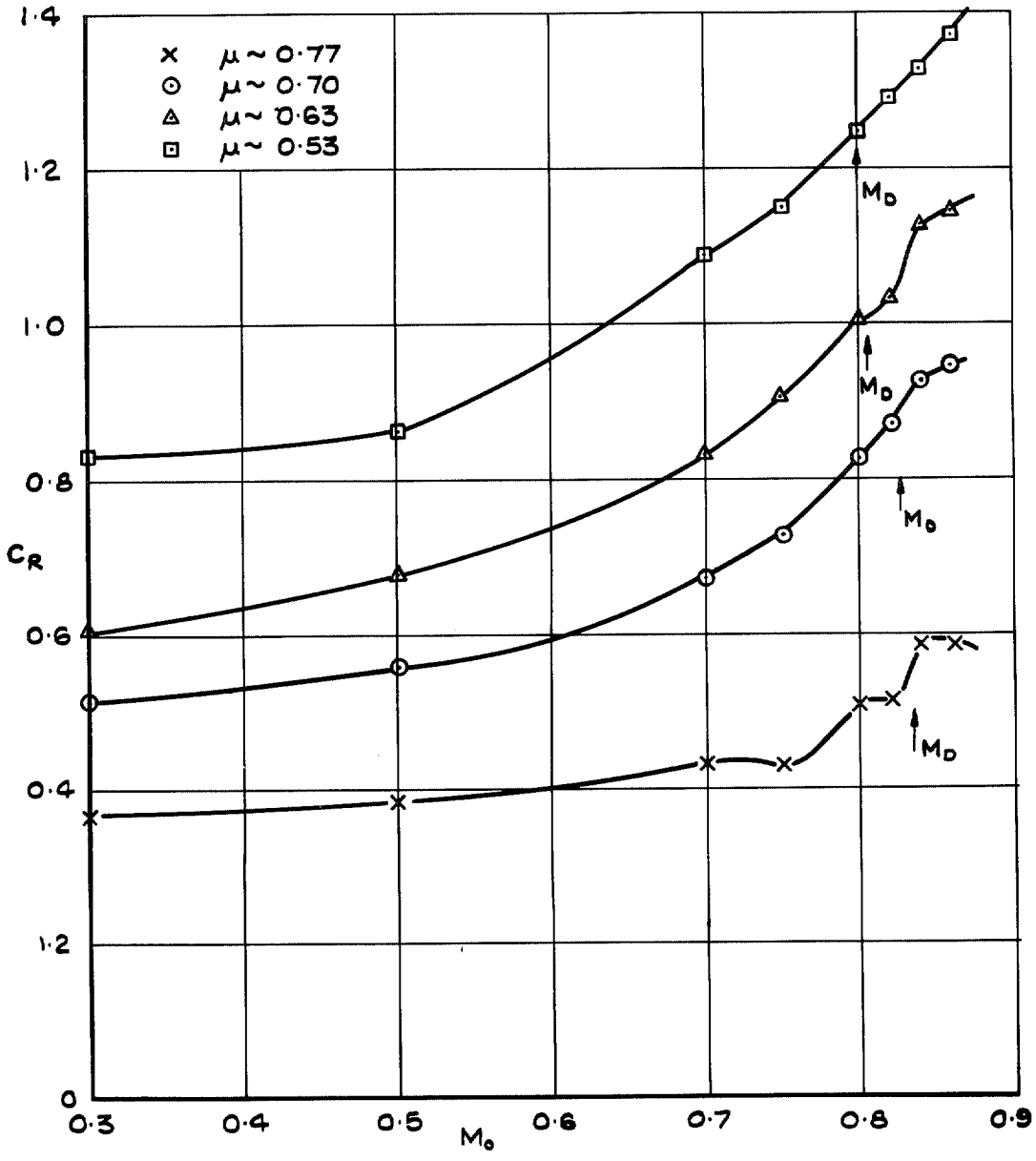


FIG. 31. Radial force coefficient $v$ Mach number: cowl 3.

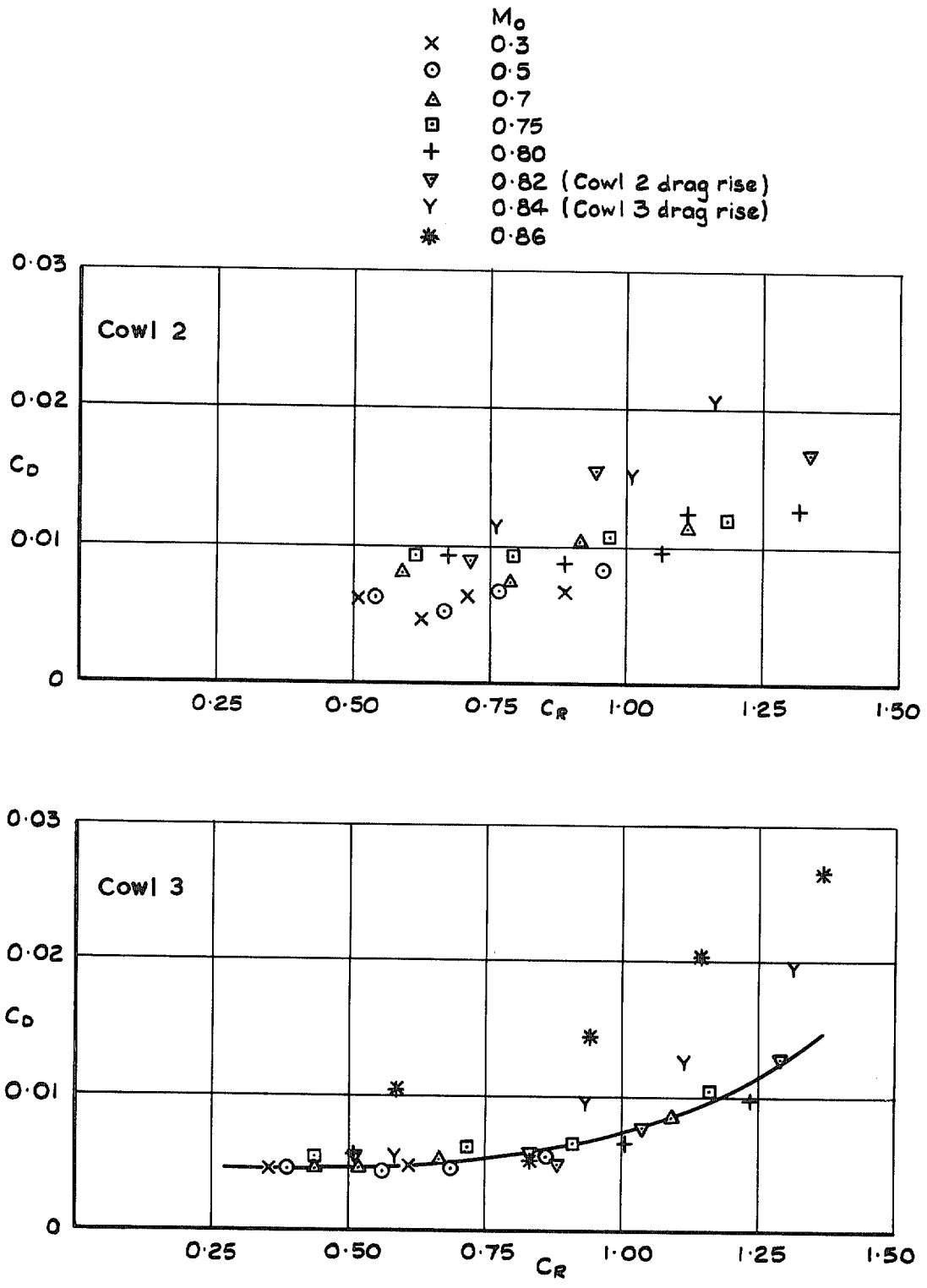


FIG. 32. External drag coefficient $v$ radial force coefficient: cowls 2 and 3.

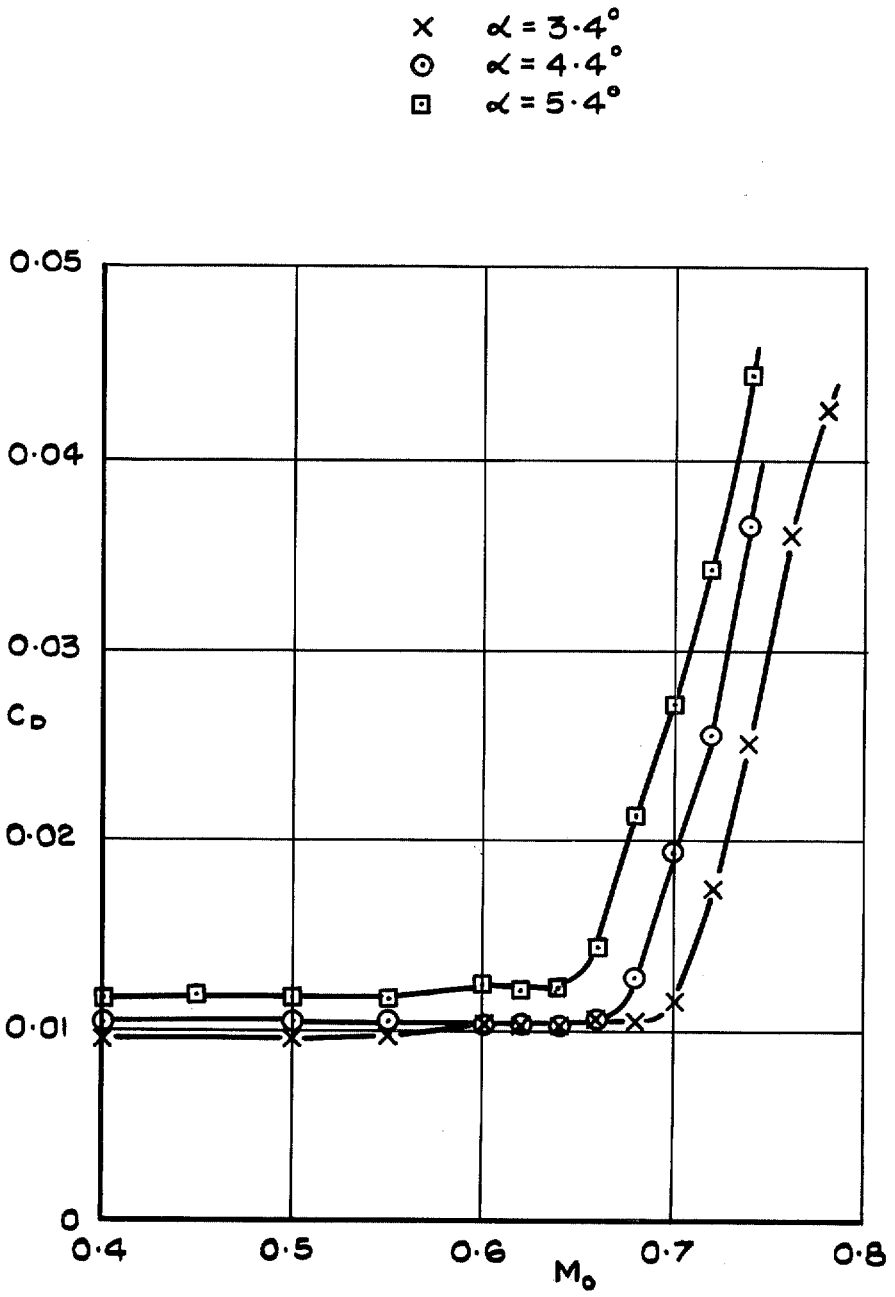


FIG. 33. Drag coefficient $v$ Mach number; aerofoil N.P.L. 3131.

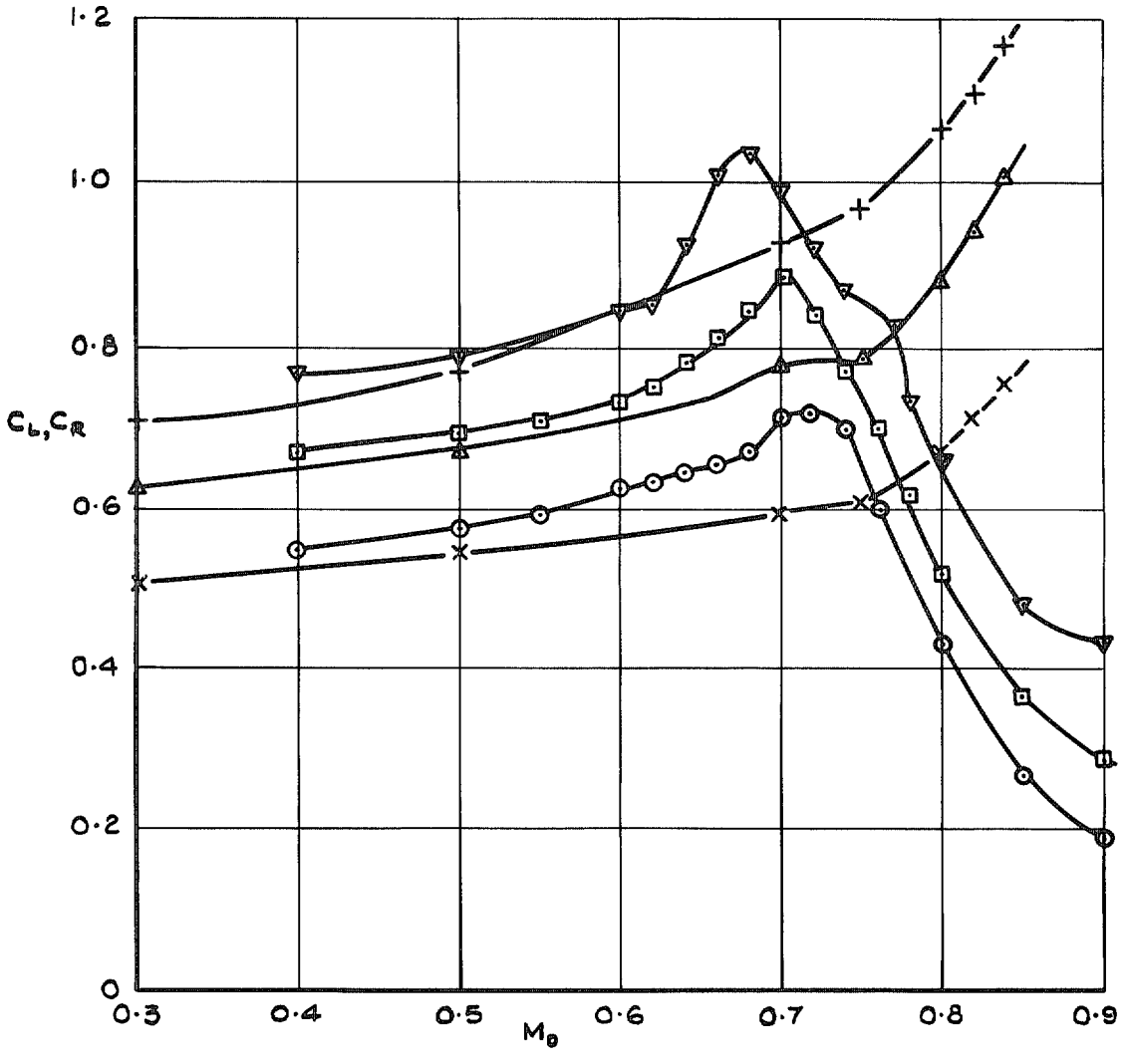


FIG. 34. Comparison between the radial force coefficient of cowl 2 and the lift coefficient of the aerofoil.

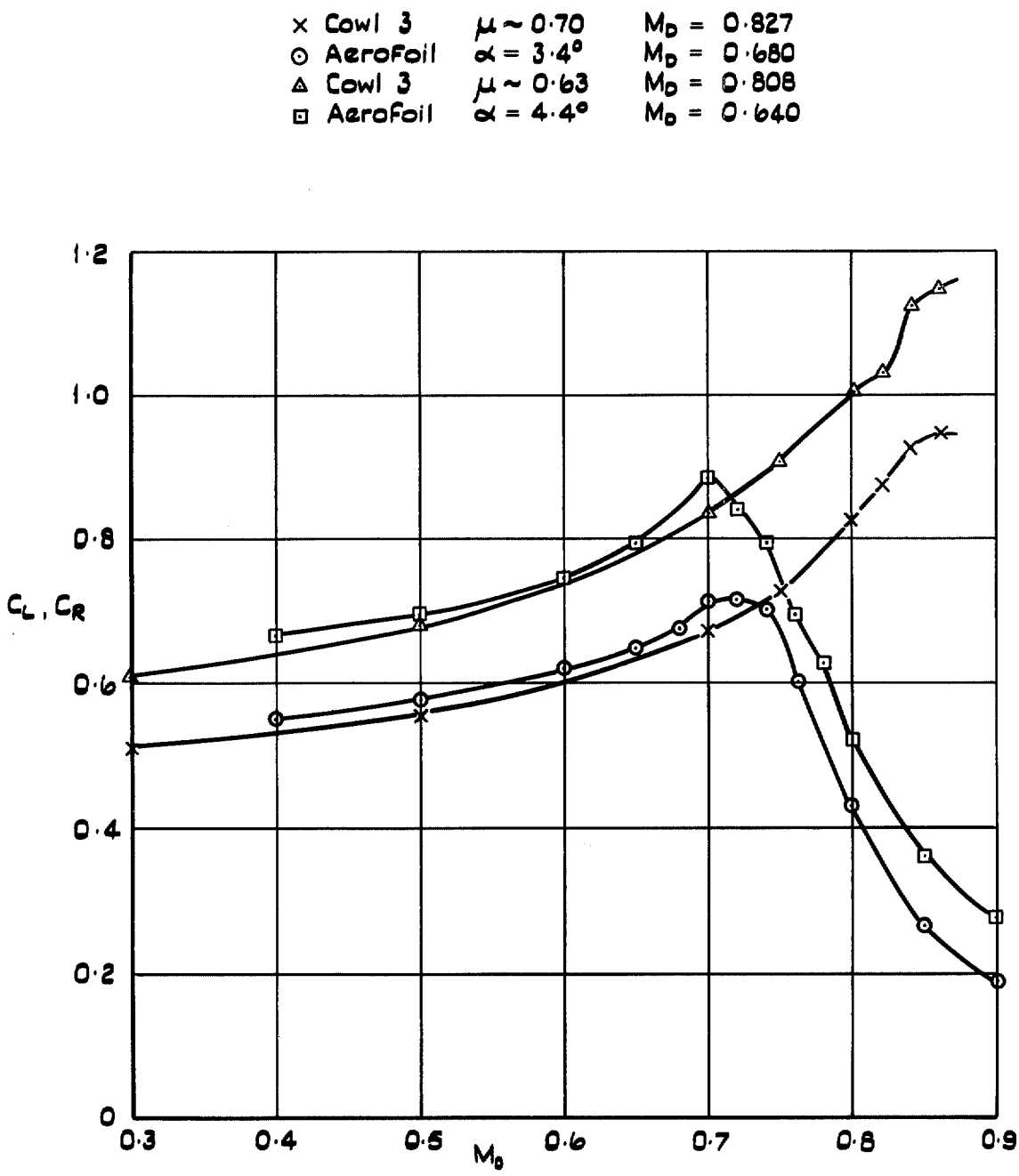


FIG. 35. Comparison between the radial force coefficient of cowl 3 and the lift coefficient of the aerofoil.

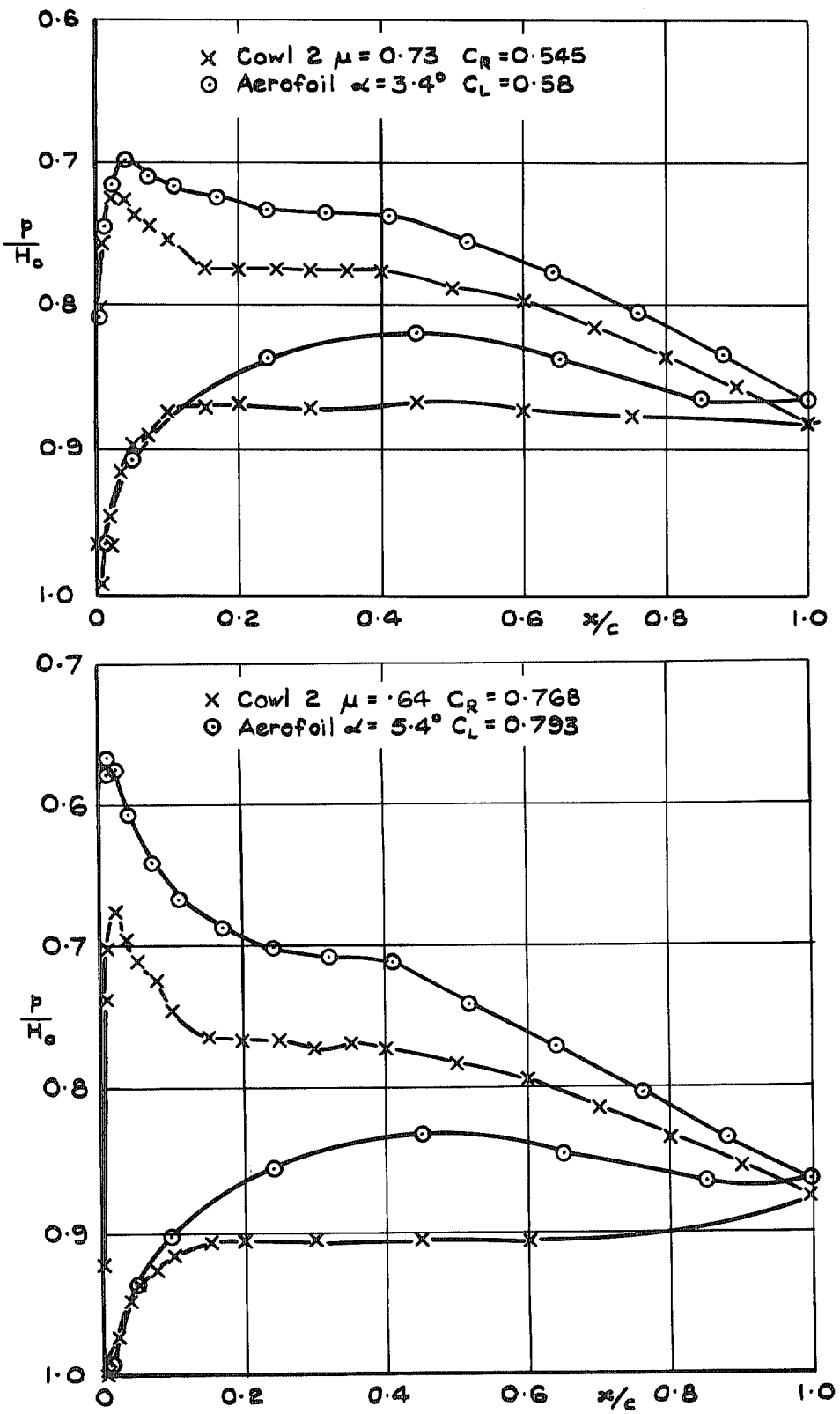


FIG. 36. Comparison between the pressure distributions measured on cowl 2 and the aerofoil at moderate Mach number.

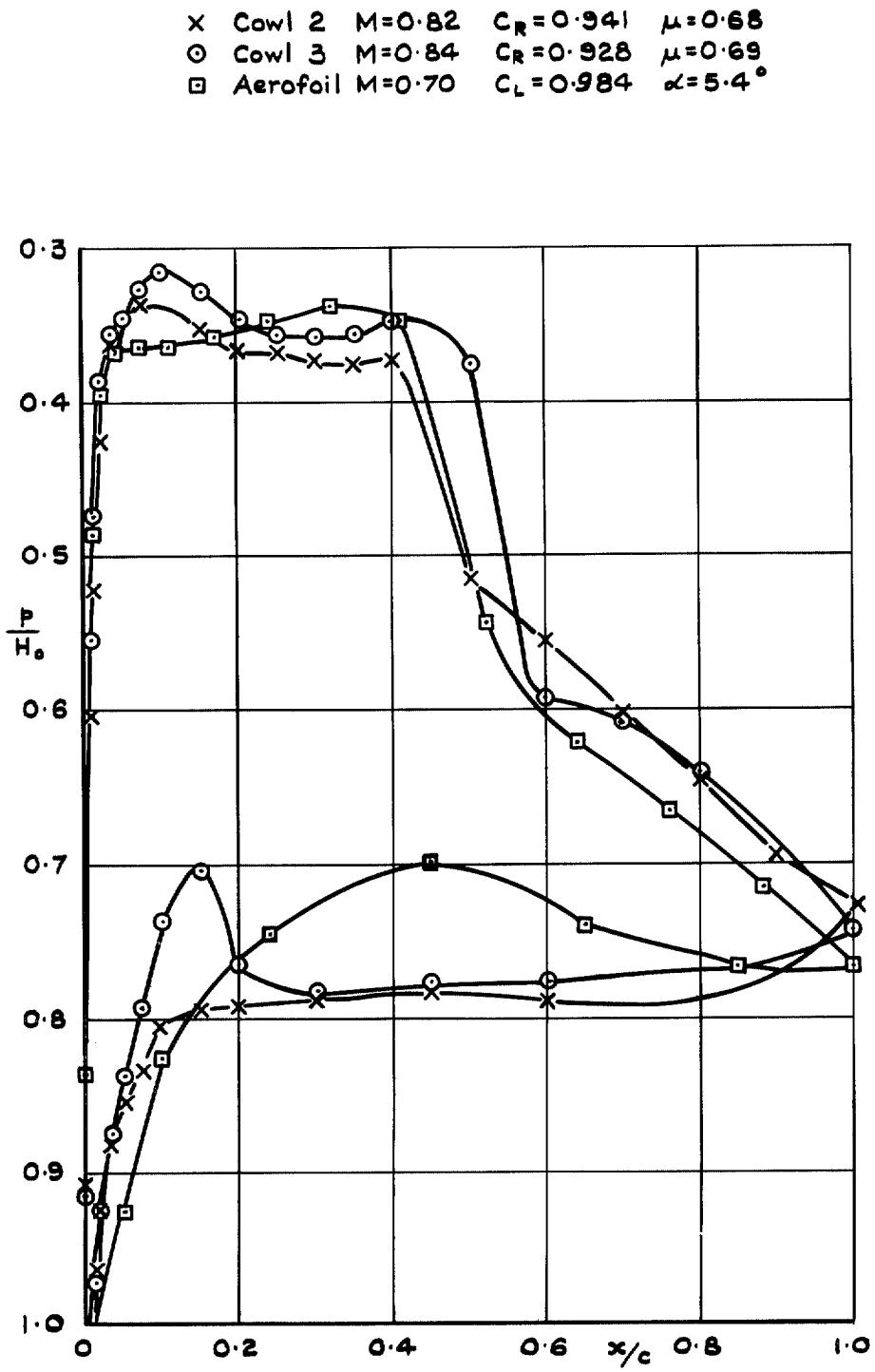


FIG. 37. Comparison between the pressure distributions measured on the cowls and the aerofoil just beyond the drag-rise Mach number.

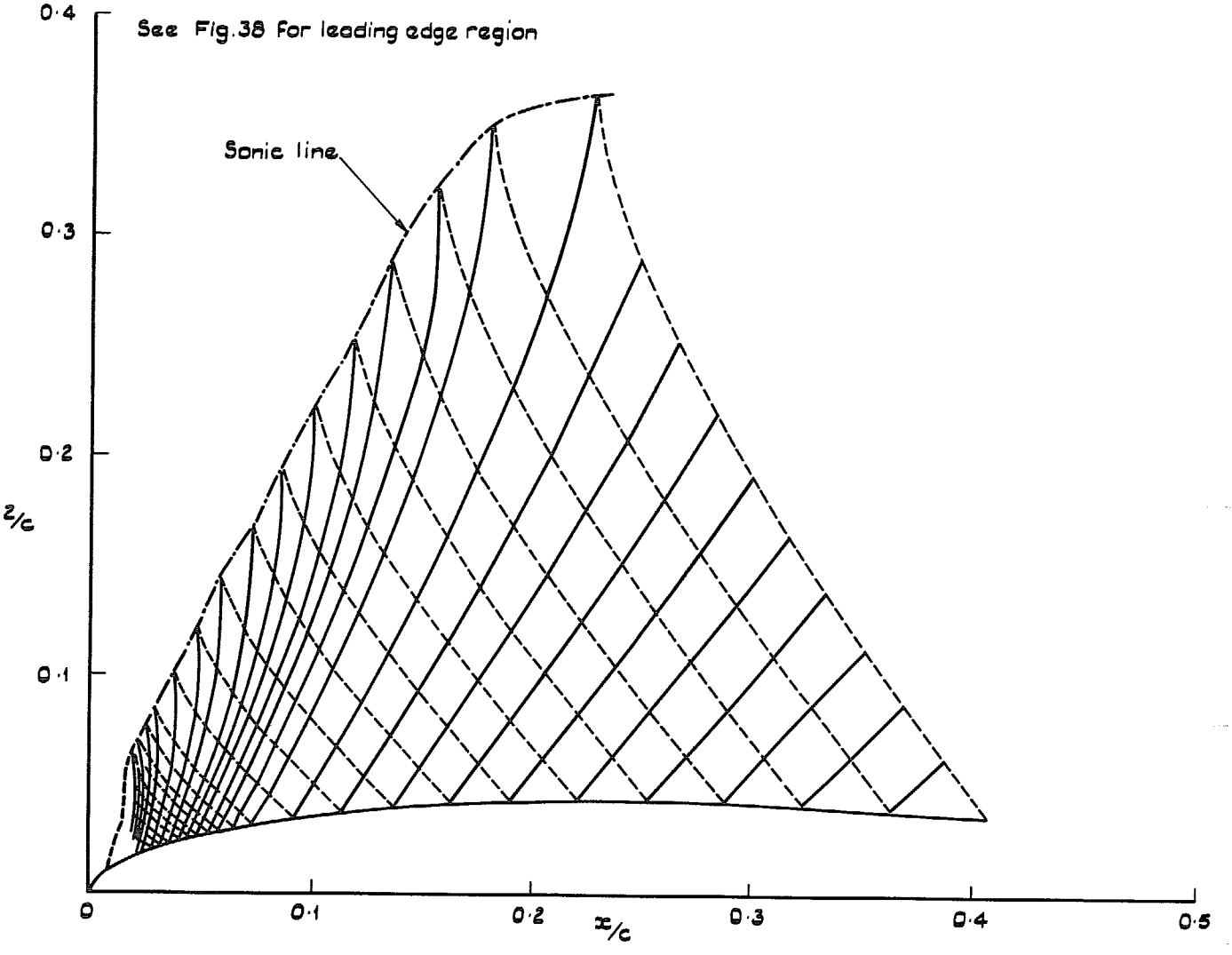


FIG. 38. Calculated characteristic mesh; aerofoil; $M = 0{\cdot}70$; $\alpha = 5{\cdot}4°$.

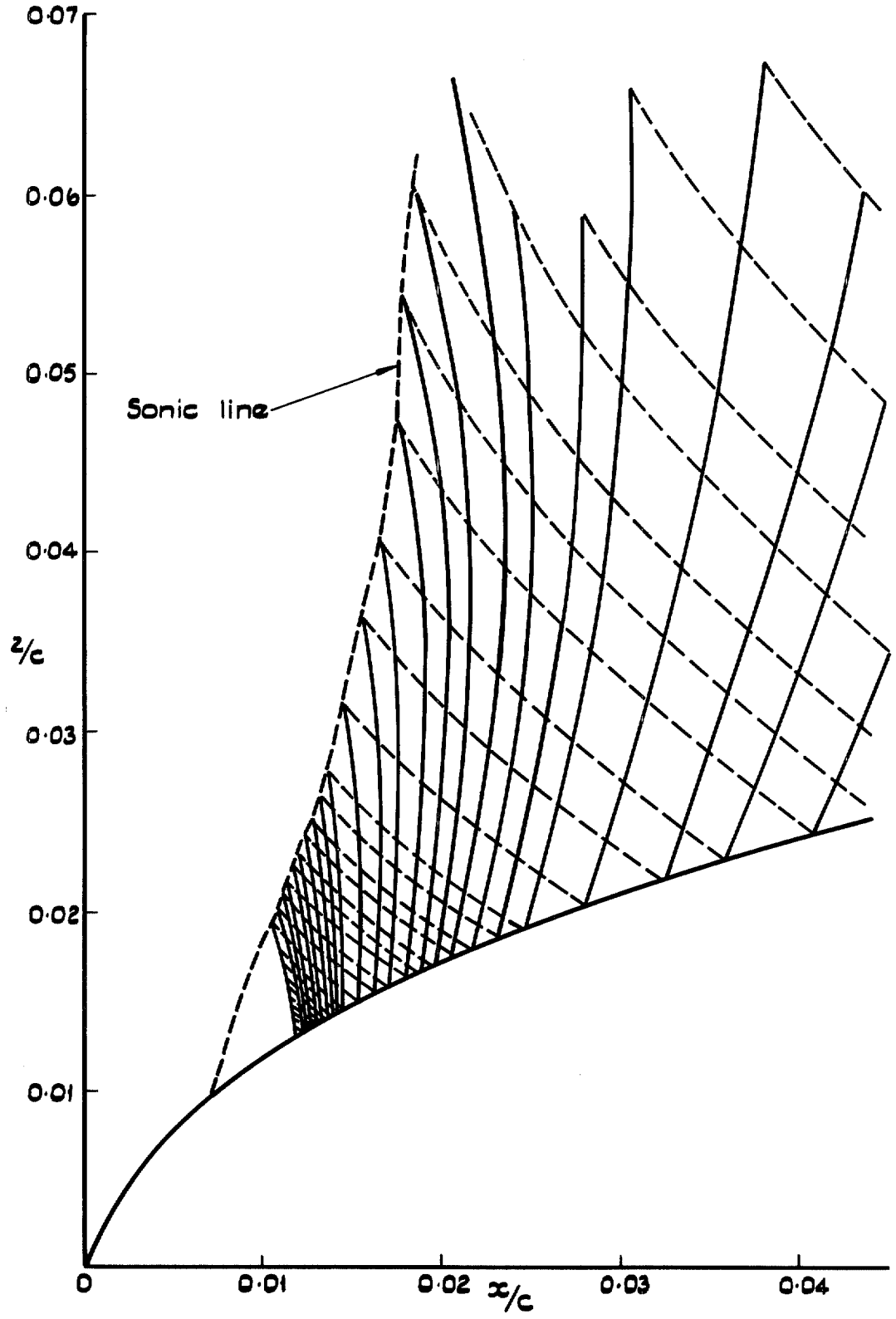


FIG. 39. Calculated characteristic mesh near the leading edge of the aerofoil: $M = 0{\cdot}70; \alpha = 5{\cdot}4°$.

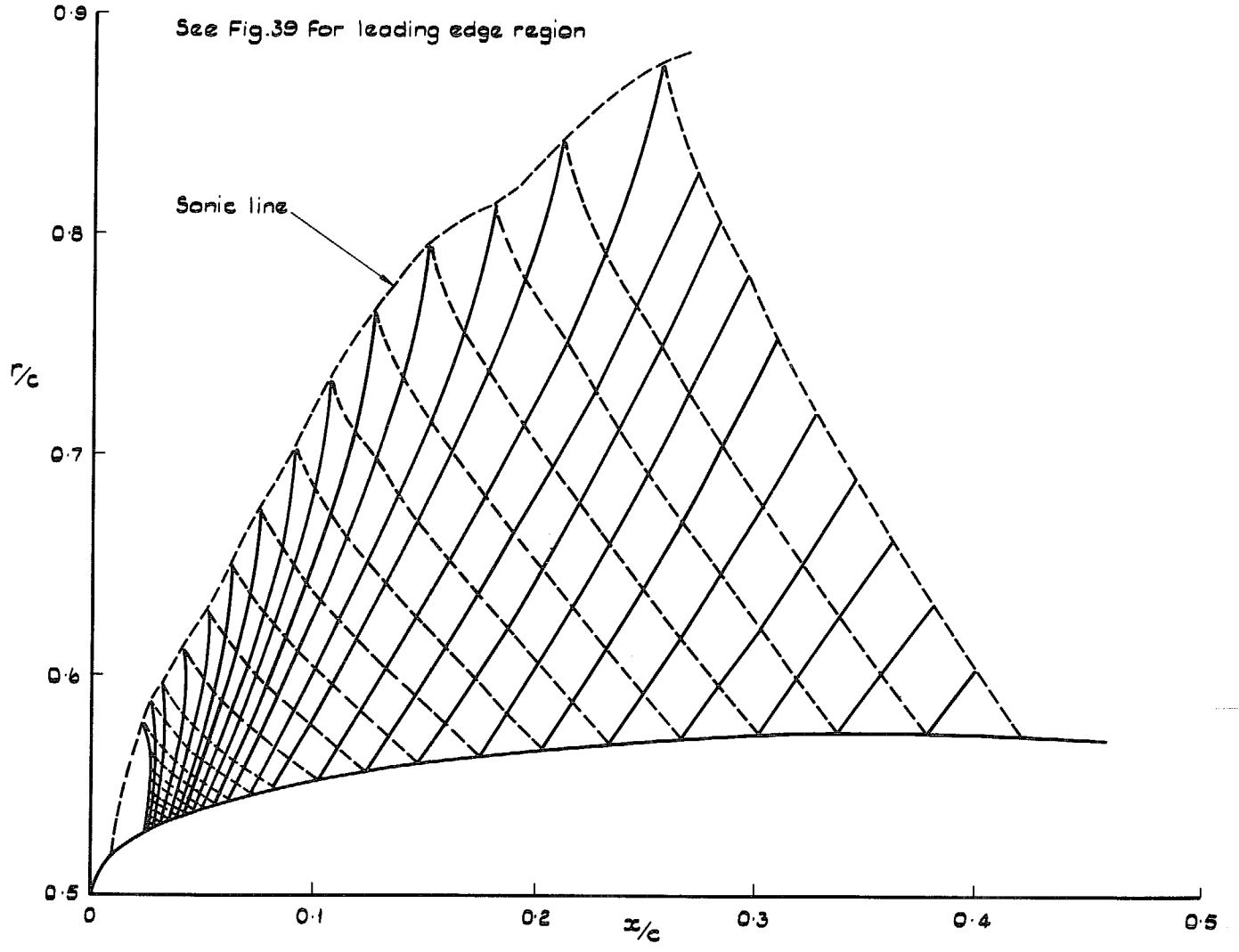


FIG. 40. Calculated characteristic mesh; cowl 2; $M = 0{\cdot}82$; $\mu = 0{\cdot}68$.

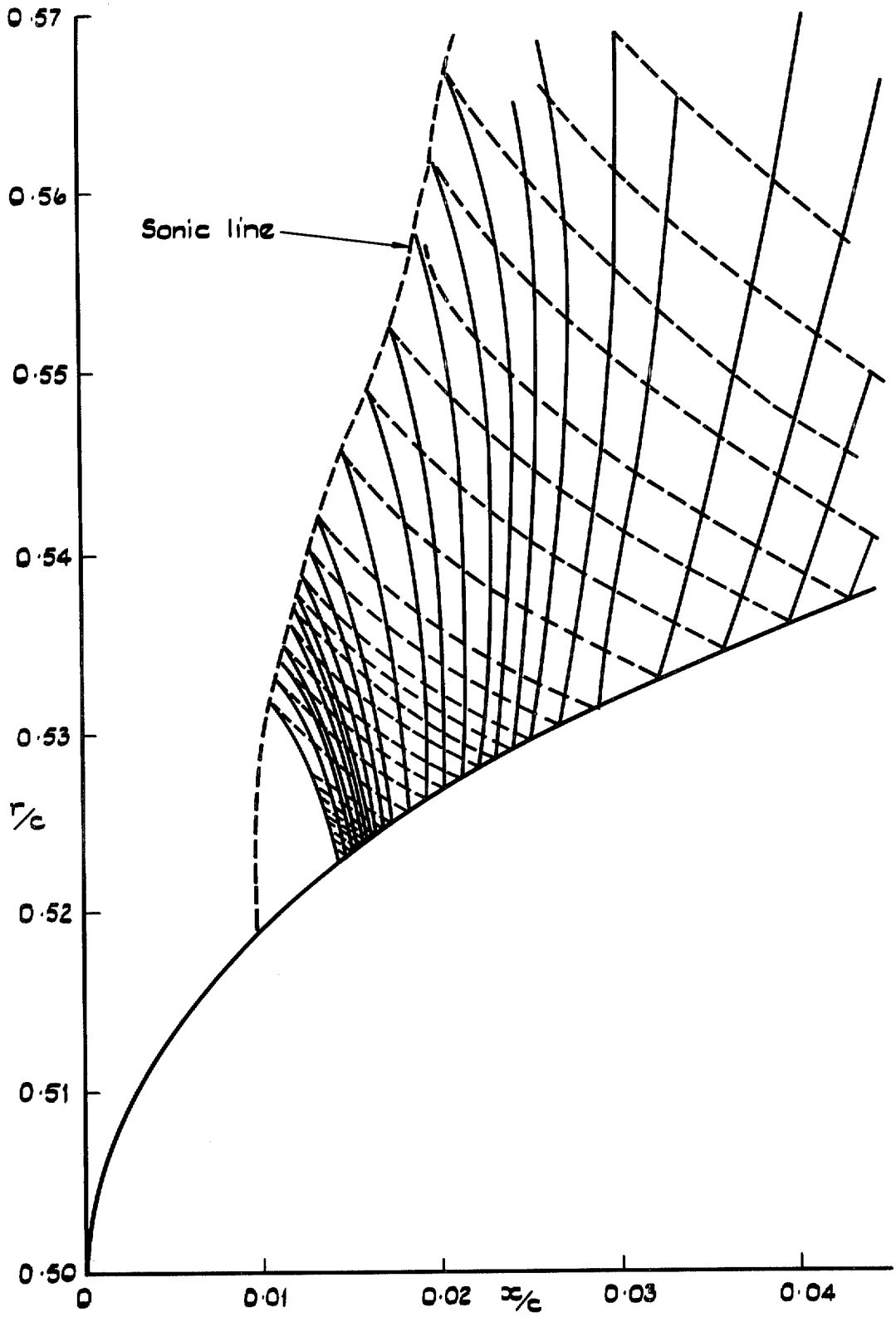


FIG. 41. Calculated characteristic mesh near the leading edge of cowl 2; $M = 0{\cdot}82$; $\mu = 0{\cdot}68$.

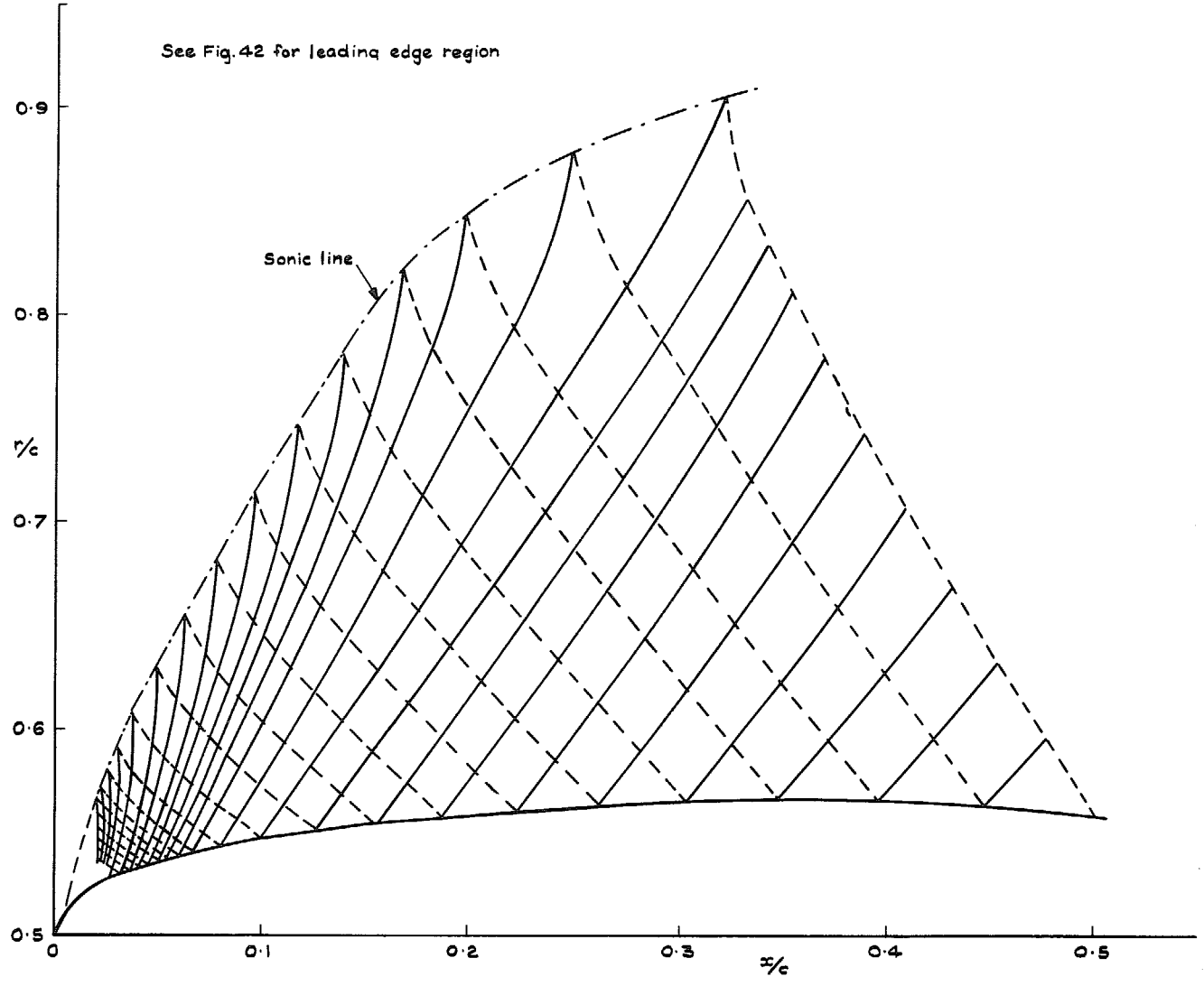


FIG. 42. Calculated characteristic mesh; cowl 3; $M = 0{\cdot}84$; $\mu = 0{\cdot}69$.

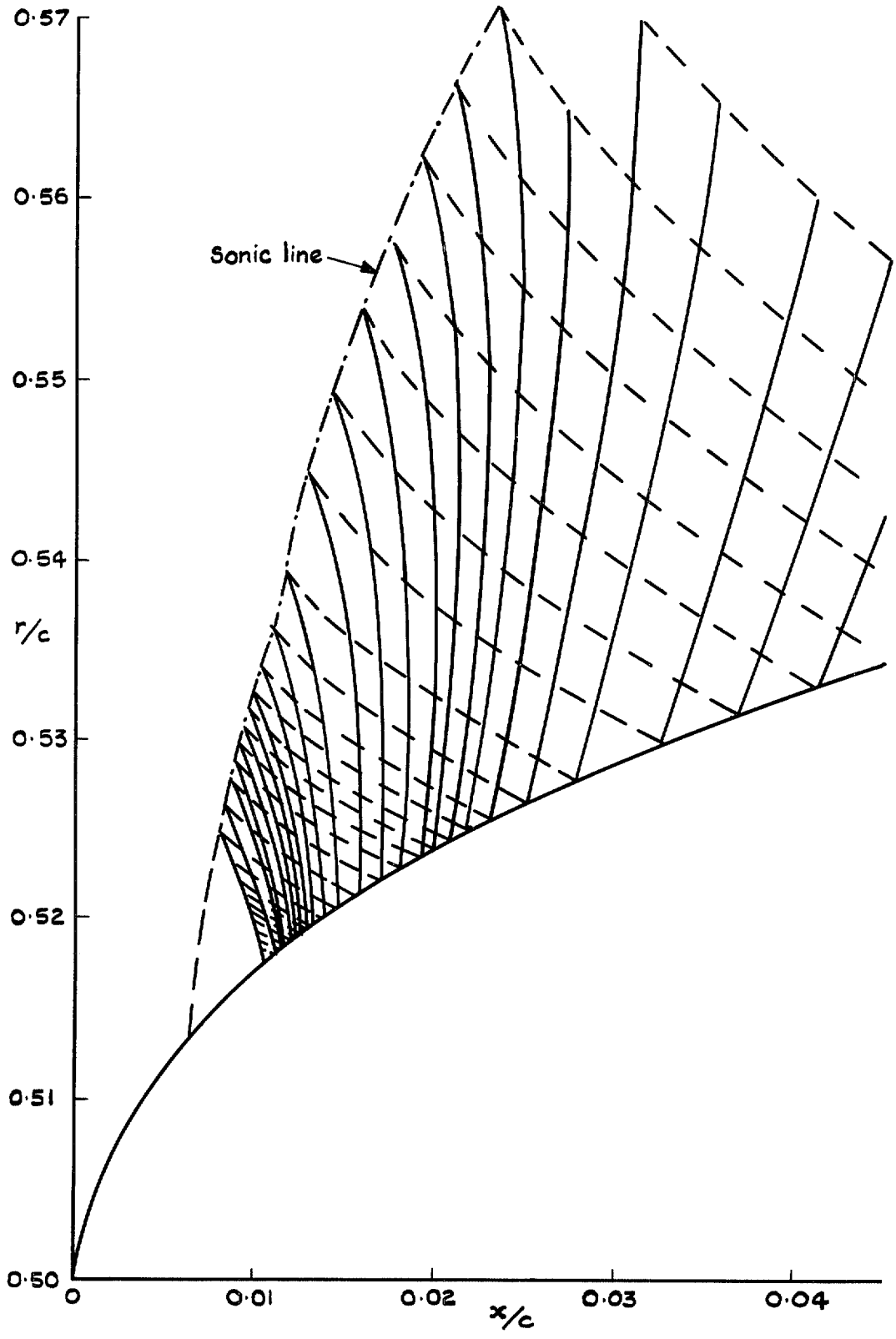


FIG. 43. Calculated characteristic mesh near the leading edge of cowl 3; $M = 0{\cdot}84$; $\mu = 0{\cdot}69$.

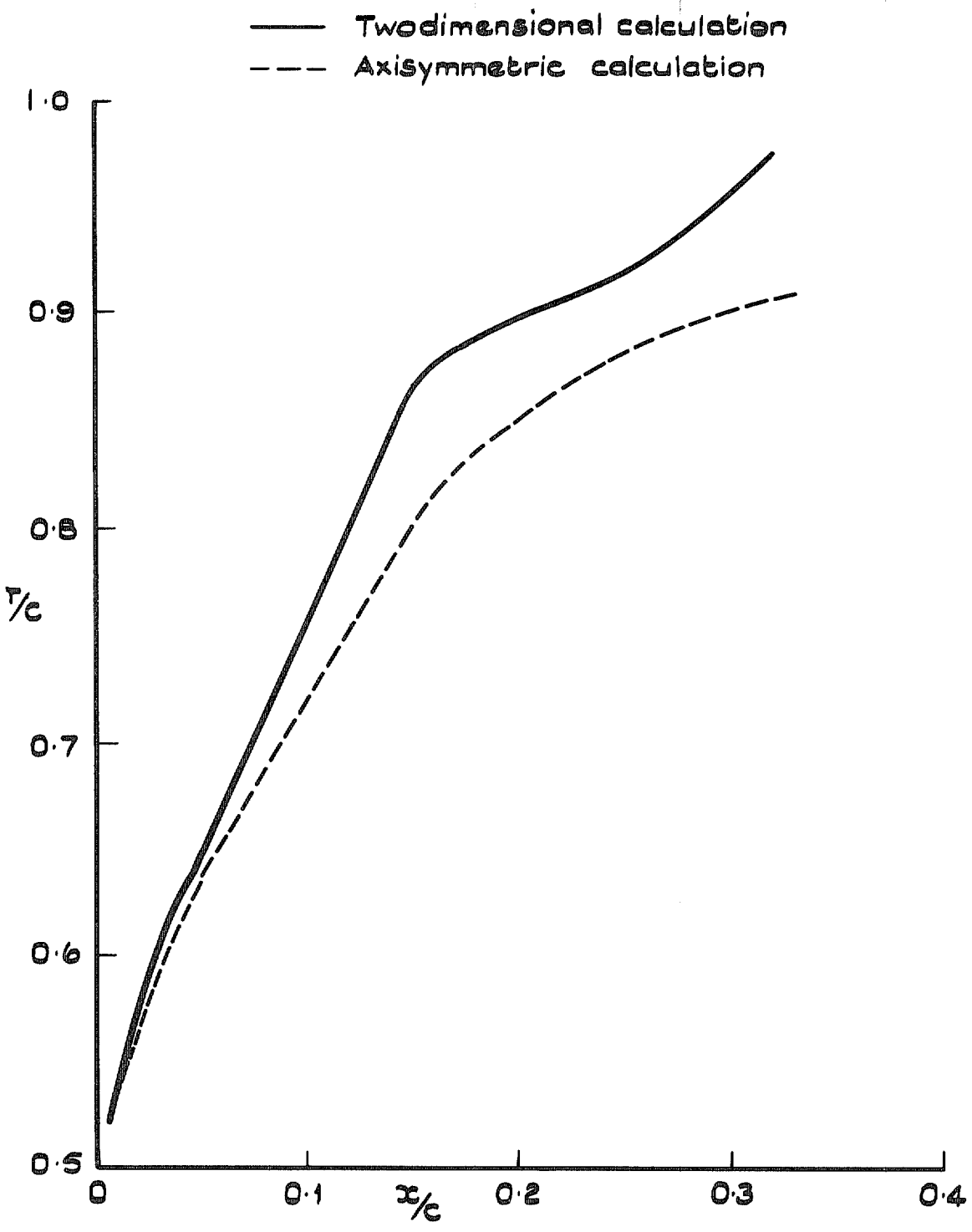


FIG. 44. Comparison of the sonic line shape calculated by axisymmetric and two-dimensional characteristics for the same pressure distribution.

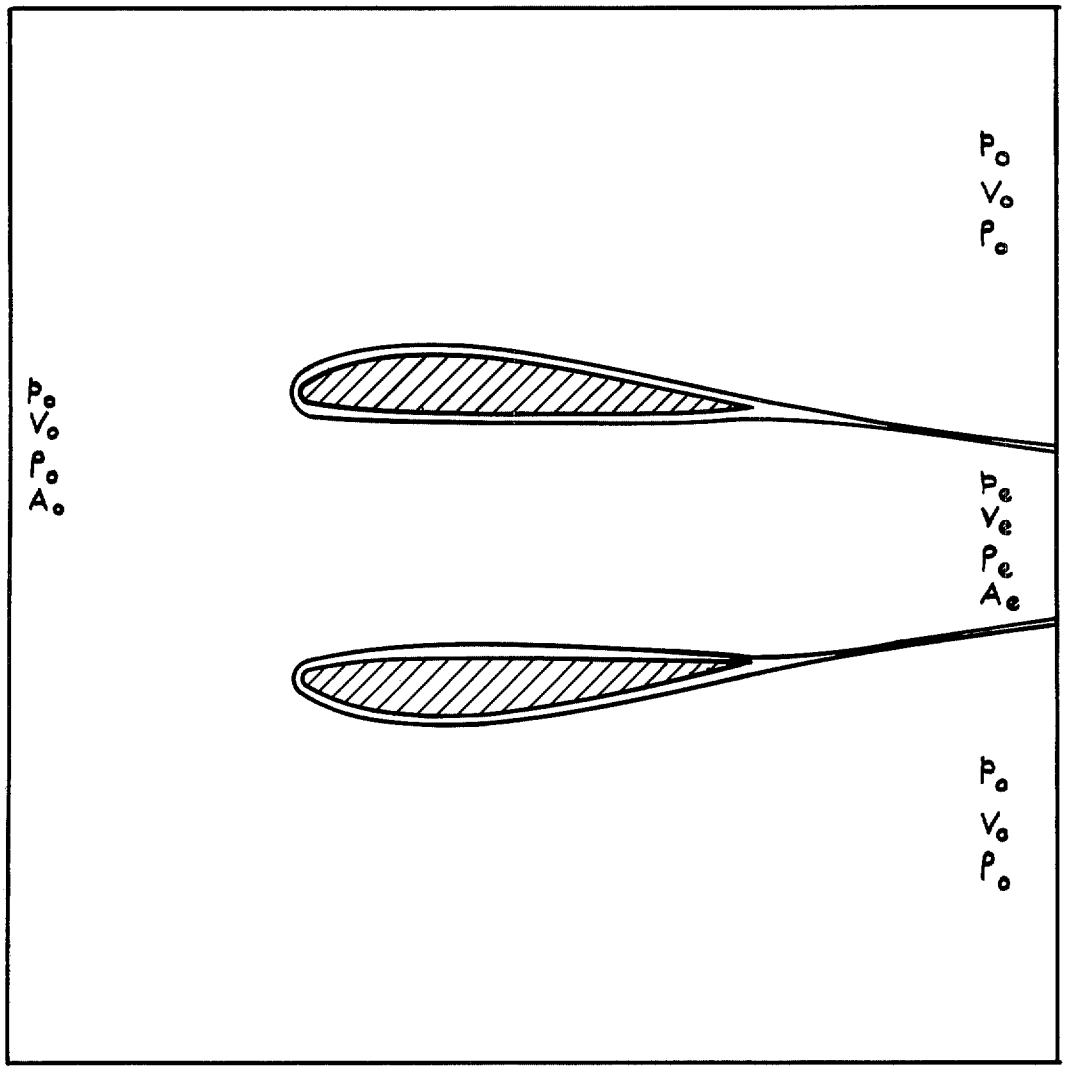


FIG. 45. Surface of integration for momentum balance.

Printed in England for Her Majesty's Stationery Office by J. W. Arrowsmith Ltd., Bristol
Dd. 503426 K5 1/73.

HER MAJESTY'S STATIONERY OFFICE

*Government Bookshops*

49 High Holborn, London WC1V 6HB
13a Castle Street, Edinburgh EH2 3AR
109 St Mary Street, Cardiff CF1 1JW
Brazennose Street, Manchester M60 8AS
50 Fairfax Street, Bristol BS1 3DE
258 Broad Street, Birmingham B1 2HE
80 Chichester Street, Belfast BT1 4JY

*Government publications are also available through booksellers*



SBN 11 470518 6